PHYSICAL REVIEW D **95,** 095018 (2017)

# Invisible decay of the Higgs boson in the context of a thermal and nonthermal relic in MSSM

Rahool Kumar Barman,[1,*] Genevieve Bélanger,[2,†] Biplob Bhattacherjee,[1,‡] Rohini Godbole,[1,§] Gaurav Mendiratta,[1,5,‖] and Dipan Sengupta[3,4,¶]

[1]*Center for High Energy Physics, Indian Institute of Science, Bangalore 560012, India*
[2]*LAPTh, Université Savoie Mont Blanc, CNRS, B.P. 110, F-74941 Annecy Cedex, France*
[3]*Department of Physics and Astronomy, Michigan State University, 567 Wilson Road, East Lansing, Michigan 48824, USA*
[4]*Laboratoire de Physique Subatomique et de Cosmologie, Université Grenoble-Alpes, CNRS/IN2P3, 53 Avenue Des Martyrs, F-38026 Grenoble, France*
[5]*Salk Institute for Biological Studies, 10010 N Torrey Pines Road, La Jolla, California 92037, USA*

(Received 17 March 2017; published 19 May 2017)

We study the decay of 125 GeV Higgs boson to a pair of lightest neutralinos in the phenomenological minimal supersymmetric standard model in the context of collider searches and astrophysical experiments. We consider the parameter space for light neutralinos that can be probed via the invisible Higgs decays and Higgsino searches at the ILC. We consider the cases where the light neutralino is compatible with the observed relic density or where the thermal relic is overabundant, pointing to nonstandard cosmology. In the former case, when the neutralino properties give rise to underabundant relic density, the correct amount of relic abundance is assumed to be guaranteed by either additional dark matter particles or by nonthermal cosmology. We contrast these different cases. We assess what astrophysical measurements can be made, in addition to the measurements made at the ILC, which can provide a clue to the nature of the light neutralino. We find that a number of experiments, including Xenon-nT, PICO-250, and LZ, in conjunction with measurements made at the ILC on invisible Higgs width can pin down the nature of this neutralino, along with its cosmological implications. Additionally, we also point out potential LHC signatures that could be complementary in this region of parameter space.

DOI: 10.1103/PhysRevD.95.095018

## I. INTRODUCTION

Particle physics today is at a juncture where all predicted particles within the Standard Model (SM) have been observed at particle colliders while no particles beyond the SM (BSM) have been detected. We have discovered a Higgs boson consistent with the properties of the SM [1,2]. The current data, however, still leave enough space for the Higgs to have nonstandard decays [3]. One such possibility is that the Higgs acts as a portal to BSM physics at the electroweak scale. An exciting prospect in this regard is to consider the Higgs decaying to a pair of invisible particles in a BSM theory. Such invisible particles, if stable at the time scale of the universe, could also be the dark matter (DM) particle. Prospects for the discovery of an invisible branching ratio of the Higgs at the LHC have been explored in a number of studies, e.g., [4–13]. In fact, both CMS and ATLAS have looked, in both Run I and Run II of LHC, for such invisibly decaying Higgs through its inclusive production in the gluon fusion, in the vector boson fusion mode, as well as in the associated production of a Higgs with a $Z$ boson. CMS has analyzed the data corresponding to 5.1, 19.7, and 2.3 fb$^{-1}$ of integrated luminosity, collected at $\sqrt{s} = 7, 8$, and 13 TeV, respectively, and has obtained an upper limit on the invisible branching fraction ∼24% at 95% C.L. [14–16]. ATLAS has also searched for the invisible decay of the Higgs boson, produced via the associated production of the Higgs with a $Z$ and via vector boson fusion [17,18]. The observed upper limit by ATLAS from the 8 TeV data corresponding to an integrated luminosity of 20.3 fb$^{-1}$ using the vector boson fusion mode on Br($h \to$ invi) is ∼28% at 95% C.L. [18]. The CMS (ATLAS) studies for the high luminosity LHC [19] project that one could reach sensitivities for the invisible branching ratio of the Higgs in the range 17%–28% (23%–32%) for 300 fb$^{-1}$ and 6%–17% (8%–16%) for 3000 fb$^{-1}$ of integrated luminosity for the production of the Higgs in association with a $Z$. More recent studies, performed for the future collider workshop [20–22], possibly reach values as low as 9%(8%) at 95% C.L. for 3000 fb$^{-1}$ at CMS (ATLAS). It should be noted, however, that these smaller numbers are usually arrived at by assuming a projected reduction in both the systematic and the theoretical errors. The more conservative limits assuming the same systematic

*rahoolkbarman@chep.iisc.ernet.in
†belanger@lapth.cnrs.fr
‡biplob@chep.iisc.ernet.in
§rohini@chep.iisc.ernet.in
‖gauravm.137@gmail.com
¶dipan@pa.msu.edu

 

errors as in the current analysis, for CMS for example, are around 21% and 20% for 300 and 3000 $\text{fb}^{-1}$ of integrated luminosity [23], respectively. Global fits to the Higgs coupling data can also probe the invisible branching ratio *indirectly*; see, e.g., [24]. These limits are usually much stronger than those given by the "direct" searches mentioned above, and it is projected that one can reach a sensitivity of about 5% [22] at the high luminosity LHC. It should be noted, however, that in this way of restricting the *invisible* branching ratio, truly invisible decays are not distinguished from other undetected decay modes. Further, these limits are subject to assumptions on the total Higgs decay width, which when modified can lead to different results. Hence the limits given by *direct* searches for an invisibly decaying Higgs boson are more model independent and less ambiguous. $e^+e^-$ colliders offer the best possibility of probing such an invisible decay mode. The future linear collider ILC offers the possibility to probe the invisible Higgs branching as low as 0.4% directly [25]. The question then naturally arises whether such precise measurements will be sufficient to probe light DM models (here light refers to $m_{\rm DM} \lesssim m_h/2$).

In $R$-parity conserving supersymmetry (SUSY), the lightest stable SUSY particle (LSP), typically the neutralino $\chi_1^0$, naturally provides a DM candidate. When the neutralino LSP is light enough, $m_{\rm DM} \lesssim M_h/2$, the Higgs has an invisible decay width into a pair of neutralinos. There exist a number of studies addressing the question of Higgs decaying invisibly to light neutralinos [26–38]. Thus there is a direct connection between invisible Higgs, DM, and collider signatures in SUSY. In Higgs portal scenarios, a direct connection between the invisible Higgs and direct detection cross section was established, showing the importance of the invisible width for very light DM [11]. Moreover, in simple extensions of the SM, e.g., with an additional scalar singlet, the requirement of sufficient annihilation in the early universe to meet the relic density constraint means that the coupling of the LSP to the Higgs is such that it implies significant invisible width. An exception to this requirement is the special case where the mass of the DM is just below $m_h/2$. Here we wish to revisit the case of neutralino DM where similar arguments apply.

In SUSY, constrained models such as the minimal supergravity or the constrained minimal SUSY (mSUGRA/cMSSM), the Higgs mass, and SUSY searches strongly constrain any light neutralino even before imposing DM constraints [39–47]. In the agnostic, phenomenological minimally supersymmetric Standard Model (pMSSM), despite the larger number of free parameters, the combination of collider, relic abundance, and direct detection results severely restrain the possibility of a light neutralino. The argument goes as follows. Because of direct limits on charged particles, the light neutralino has to be dominantly bino. The annihilation cross section of the bino is typically not large enough to ensure compatibility with the observed relic abundance unless special mechanisms that require some specific mass relations come into play such as annihilation through a $Z$-boson, a Higgs, or a light pseudoscalar resonance [30,38,48–53] or an exchange of light sfermions [34,54–56]. Thus, generally the scenarios are fine-tuned. Recently, a number of studies have considered the status of the pMSSM post 7 and/or 8 TeV runs of the LHC [28,29,35,46,57–66] and more specifically of the light neutralino. It was found that a light neutralino in the pMSSM models is generally constrained to masses above $\approx$30 GeV [35,59,64] in order to avoid an overabundant relic density of the DM although there remains a small window at lower masses when the model contains also very light sleptons or sbottoms that may escape the LEP limits [56,67]. These light neutralinos can lead to a large branching ratio for the Higgs decaying to invisible particles [59] and can be further probed in direct detection [53], as well as in a collider environment.

Clearly, the precise determination of the DM relic abundance plays a crucial role in constraining light neutralino DM. However, the constraints are only valid within the framework of a standard cosmological scenario which assumes that neutralinos have been produced thermally and were in thermal equilibrium with SM particles in the early universe before they decouple at a freeze-out temperature $T_F \approx m_{\rm DM}/20$. Going beyond the simplest assumption of the standard cosmological scenario, or more generally not requiring that all the DM be explained by the freeze-out mechanism, will clearly open up the possibility for light DM in the MSSM. Such scenarios are characterized by a late decaying heavy field, for example, a SUSY modulus scalar [68]. Depending on whether a DM candidate in the conventional, thermal freeze-out scenario is underabundant or overabundant, the nonthermal mechanisms by which one attains the observed relic density vary [69]. In SUSY with overabundant DM (for example, binolike DM), the late decay of a SUSY modulus scalar field dilutes the entropy density of the universe. As long as the branching fraction of the decaying scalar into DM is not too large, the observed relic density can be reproduced for almost all values of scalar mass and reheating temperature ($T_{RH} > T_{BBN}$) [69,70]. In the case of thermally underabundant DM too, late decay of a scalar can lead to the correct relic abundance. Thus, both underabundant and overabundant DM in the thermal freeze-out picture can be brought into agreement with the observed DM abundance. Note, of course, that in the former case there exists the possibility that instead of the late decaying scalar it is the existence of multicomponent DM that guarantees the correct relic density.

Given the sensitivity of future experiments, both collider and astrophysical, it is thus important to reassess the possibility of discovery of nonthermal light dark matter within the framework of the MSSM. Some studies of nonthermal dark matter in MSSM have been conducted

[69,71–73]. The issue of how one can distinguish thermal and nonthermal mechanisms by exploiting the complementarity between various experiments has begun to be explored; see, e.g., [74]. Our goal here is to provide a comparative study of the status of light neutralino dark matter in the MSSM within both the thermal and the nonthermal regimes. We will consider mainly two types of scenarios: in the first, dubbed thermal DM, we assume the standard cosmological scenario but allow the DM to be underabundant; the underlying assumption is that another particle would form a second DM component or there exists an underlying nonthermal mechanism that brings the relic density of an otherwise underabundant DM in agreement with the observed value. In the second scenario, we concentrate on the case where thermal production of DM leads to overabundance which clearly calls for a nonstandard mechanism. In this case we call it a nonstandard cosmological dark matter (NSDM) scenario.

In the framework of the MSSM, we define the parameter space compatible with both classes of DM scenarios. We will show that including the possibility of nonthermal DM cosmology opens up the region with a light neutralino which can therefore contribute to invisible Higgs decays. After defining the currently allowed parameter space, we find the reach for the ILC to probe the remaining parameter space through either Higgs invisible decays or direct production of charginos/neutralinos and explore the implications for present and future direct detection experiments in both spin dependent and independent searches. We further investigate the complementarity of the different collider and direct detection searches to probe the light neutralino scenarios. We shall also address the question of what additional signatures one could primarily focus on at the LHC to achieve this goal, and whether such a signal, in conjunction with the above observations, can decipher the nature of the dark matter particle. We also provide a roadmap for the experimental searches for a light neutralino in the MSSM for different possible cosmological histories of DM.

This paper is organized as follows. In Sec. II, we define the free parameters of the model and the basic collider constraints including LEP limits, flavor observables, and Higgs physics. In Sec. III, we reinterpret the null results of searches for electroweakinos at the LHC. The results of the scan of the parameter space for scenarios with a thermal DM that is not overabundant are presented in Sec. IV, while Sec. V includes all NSDM scenarios. Section VI discusses the potential to probe light neutralinos at ILC and in direct detection. In Sec. VII, we briefly discuss the role of high luminosity LHC in probing light neutralino DM. We finally conclude in Sec. VIII.

## II. MODEL, PARAMETER SPACE, AND CONSTRAINTS

We work within the framework of the MSSM with parameters defined at the electroweak scale. Since our main focus is the physics of the Higgs and electroweakino sectors, we consider only the nine parameters that capture the relevant physics: the gaugino masses $M_1$, $M_2$, the Higgsino mass, $\mu$, the ratio of the Higgs vacuum expectation values, $\tan\beta$, the mass of the third generation squarks, $m_{\tilde{Q}_3}$ ($m_{\tilde{Q}_{3l}}, m_{\tilde{t}_R}, m_{\tilde{b}_R}$), the trilinear coupling of the stop $A_t$, and the mass of the gluino $M_3$. The first four parameters determine the electroweakino masses and couplings while the latter three enter the higher-order corrections to the Higgs mass. Note that the mass of the third generation squarks, $m_{\tilde{Q}_{3l}}$, $m_{\tilde{t}_R}$, and $m_{\tilde{b}_R}$, have been independently varied between 800 GeV and 10 TeV. The two couplings that will be most relevant for our study are those of the LSP to the Higgs and to the $Z$ boson. Both the couplings play a role in computing the dark matter observables, while the former also determines the invisible width of the Higgs boson. These couplings are defined

$$g_{Z\tilde{\chi}_1^0\tilde{\chi}_1^0} = \frac{g}{2\cos\theta_W}(|N_{13}|^2 - |N_{14}|^2),$$
$$g_{h\tilde{\chi}_1^0\tilde{\chi}_1^0} = g(N_{11} - \tan\theta_W N_{12})(\sin\alpha N_{13} + \cos\alpha N_{14}), \quad (2.1)$$

where $g$ is the SU(2) coupling, $\alpha$ is the Higgs mixing angle, and $N_{1i}$ are elements of the neutralino mixing matrix with $N_{11}$ and $N_{12}$ representing the bino and wino components, respectively, while $N_{13}$, $N_{14}$ are representatives of the Higgsino components.

We explore the reduced nine-dimensional parameter space of the MSSM with a random scan within the following ranges:

$$1\ \text{GeV} < M_1 < 100\ \text{GeV}, \quad 90\ \text{GeV} < M_2 < 3\ \text{TeV},$$
$$1 < \tan\beta < 55, \quad 70\ \text{GeV} < \mu < 3\ \text{TeV},$$
$$800\ \text{GeV} < m_{\tilde{Q}_{3l}} < 10\ \text{TeV}, \quad 800\ \text{GeV} < m_{\tilde{t}_R} < 10\ \text{TeV},$$
$$800\ \text{GeV} < m_{\tilde{b}_R} < 10\ \text{TeV}, \quad 2\ \text{TeV} < M_3 < 5\ \text{TeV},$$
$$-10\ \text{TeV} < A_t < 10\ \text{TeV}. \quad (2.2)$$

Note that the mass of the gluino is assumed to be large in order to safely avoid strong constraints from the LHC. Similarly the masses of the first and second generation squarks, $m_{\tilde{Q}_{2l},\tilde{Q}_{1l},\tilde{c}_{L,R},\tilde{s}_{L,R}}$ and the sleptons masses are fixed at 3 TeV, heavy enough to decouple from the collider phenomenology. Moreover, $A_b = A_\tau = 0$, and the pseudoscalar mass is taken to be rather heavy, $M_A = 1$ TeV. Allowing lower values for $M_A$ could impact the dark matter phenomenology, in particular by offering a new channel for efficient light neutralino annihilation through a pseudoscalar exchange [31]. A light second Higgs doublet playing a role in neutralino annihilation is, however, strongly constrained from both astrophysical measurements such as FermiLAT and LUX [55] as well as from colliders including direct searches at the LHC [75], properties of the 125 GeV Higgs boson [76] and searches for the decay

$B_s \to \mu^+\mu^-$ [77]. We generate $\approx 10^7$ parameter space points and implement the relevant constraints in order to obtain the allowed parameter space. We only consider points for which the decay of the Higgs into a pair of neutralinos is kinematically allowed.

The parameter space is initially constrained by imposing the limits on the mass of the light *CP*-even neutral MSSM Higgs boson ($h$). Note here that we impose that the lightest Higgs $h$ behaves like the SM Higgs boson with a mass of 125 GeV, with the couplings satisfying the constraints derived from the LHC. We also constrain the parameter space by imposing low energy flavor physics constraints, the limit on the invisible decay width of the $Z$ boson, LEP limits on electroweakinos, and Higgs signal strength limits derived from the LHC Run-I data, through a combined analysis by ATLAS and CMS Collaborations. These constraints are discussed in more detail below, while other constraints from direct electroweakino searches at the LHC are detailed in the next section.

(i) *Light Higgs mass*: ATLAS and CMS have performed a combined measurement of the Higgs mass ($M_h$), and its value has been determined to be in the range 124.4–125.8 GeV [78] at $3\sigma$. Taking into account the theoretical uncertainties associated with the computation of the Higgs mass, we choose a conservative approach and impose that the light Higgs mass lies within the range, $122\ \text{GeV} < M_h < 128\ \text{GeV}$. The particle spectrum is generated using SUSPECT (version 2.43) [79] and includes dominant two-loop corrections to the Higgs mass in the $\overline{\text{DR}}$ scheme.

(ii) *Flavor physics observables*: Flavor physics observables are among the most sensitive probes of new physics effects and have been extensively used to constrain BSM physics. Since the mass of the first two generations of squarks have been fixed at a high value of 3 TeV, their contributions to the rare-decay processes decouple. Thus the main contribution to $B_s \to \mu^+\mu^-$ comes from penguin diagrams with the incoming $b$ and $s$ quarks coupled to a chargino and an up-type squark. These branching fractions were obtained using micrOMEGAs (version 4.2.3) [80–82] We adopt a moderate approach here and impose the constraints on the branching fraction of $B_d \to X_s\gamma$ and $B_s \to \mu^+\mu^-$, allowing $2\sigma$ uncertainty with respect to the currently measured best-fit values: $B_d \to X_s\gamma = (3.32 \pm 0.15) \times 10^{-4}$ [83] and $B_s \to \mu^+\mu^- = 2.8^{+0.7}_{-0.6} \times 10^{-9}$ [84].

(iii) *LEP limits*: Upper limits have been derived from LEP data on the associated neutralino production cross section ($\sigma_{\tilde{\chi}_1^0\tilde{\chi}_2^0}$) times the branching fraction of $\tilde{\chi}_2^0 \to q\tilde{q}\tilde{\chi}_1^0$ [85]. An upper limit has been obtained on $\sigma_{\tilde{\chi}_1^0\tilde{\chi}_2^0} < 0.1$ pb [85] at 95% C.L., for $(|M_{\tilde{\chi}_2^0} - M_{\tilde{\chi}_1^0}| > 5\ \text{GeV})$. We implement this constraint in our analysis, and the values of the relevant variables have been obtained using micrOMEGAs (version 4.2.3) [80–82]. We also impose an upper limit on the invisible decay width of the $Z$ boson, $\Gamma_Z^{\text{inv}} < 2$ MeV [86]. Here "invisible" refers to the non-SM invisible decay modes only. In addition, we also impose a lower limit on chargino mass, $M_{\tilde{\chi}_1^\pm} < 103$ GeV [85]. This constraint implies that the lightest neutralino with a mass below $M_h/2$ is dominantly bino.

(iv) *Higgs boson width*: We also impose an upper limit on the total decay width of the Higgs boson, $\Gamma_h < 22$ MeV [87], derived by CMS at 95% C.L., using LHC data collected at $\sqrt{s} = 7$ TeV and 8 TeV corresponding to an integrated luminosity of 5.1 fb$^{-1}$ and 19.7 fb$^{-1}$, respectively.

(v) *Higgs signal strength constraints:* The Higgs boson is dominantly produced at LHC through gluon fusion ($ggF$). The other production modes are vector boson fusion ($VBF$), associated production with a vector boson ($Vh$, where $V = W, Z$), and associated production with a pair of top quarks ($t\bar{t}h$). Both ATLAS and CMS Collaborations have analyzed various final states from Higgs boson decay, such as $h \to \gamma\gamma, W^+W^-, ZZ, b\bar{b}, \tau^+\tau^-$, and have presented their results in the form of signal strength variables $\mu_f^i$, where $\mu_f^i$ is defined as the ratio of the Higgs production cross section in the $i$th production mode times the branching fraction of Higgs boson in the $f$ final state for the model under consideration, with respect to the same quantity in SM. It is expressed as

$$\mu_f^i = \frac{\sigma_i \times \text{Br}(h \to f)}{(\sigma_i \times \text{Br}(h \to f))_{\text{SM}}}. \tag{2.3}$$

Here, $i$ corresponds to the production modes of the Higgs boson, $i = ggF, VBF, Vh, t\bar{t}h$, and $f$ corresponds to the decay channel of the Higgs boson, $f = \gamma\gamma, W^+W^-, ZZ, b\bar{b}, \tau^+\tau^-$.

ATLAS and CMS have performed a combined analysis of LHC Run-I data and have presented their results in the form of two-dimensional correlation contours in the $\mu_{ggF+Vh} - \mu_{VBF+t\bar{t}h}$ plane at 68% and 95% C.L., shown in Fig. 28 of [88]. In this work, we consider only those parameter space points which lie inside the 95% C.L. correlation contours for the $\gamma\gamma, W^+W^-, ZZ, b\bar{b}, \tau^+\tau^-$ final states. Note that the currently available 13 TeV data are comparable to the 8 TeV data [89].

(vi) *Constraints from the invisible Higgs decays*: We also take into account direct search limits on the invisible decay of the Higgs boson. Direct search limits for an invisible decay mode of the Higgs in the

$Wh$, the $Zh$, and the $VBF$ channels performed by the ATLAS Collaboration using the full 7 and 8 TeV data set the upper limit to be 0.25 [17]. The CMS Collaboration similarly, by using the full 7, 8 TeV, as well as 2.3 $\text{fb}^{-1}$ data from the 13 TeV run, sets an upper limit of 0.24 from direct searches on the invisible branching ratio of the Higgs [15]. Note that in all of the above, standard model production cross section and BR are assumed. In practice, the scenarios satisfying the Higgs signal strength constraints also automatically respect the direct limit constraints.

## III. CONSTRAINTS FROM ELECTROWEAKINO SEARCHES AT THE LHC

Having documented the constraints on the electroweakino parameter space from LEP and other indirect sources in the previous section, we turn our attention to direct collider searches, focusing on the region of parameter space of interest in this study. Within the scope of this work, the LSP mass $M_{\tilde{\chi}_1^0} \leq M_h/2$ and, hence, the LEP constraints impose that the light LSP be dominantly bino. On the other hand, the relic density constraint requires that the light LSP also possess a Higgsino or wino component [30,48–53]. Since we will consider both the case of the neutralino being a standard thermal relic and the case of alternative cosmologies, for collider studies we remain agnostic to the finely tuned relic density viable regions. Within the framework of a model with heavy sfermions, the most relevant parameters are $\mu, M_1, M_2$, and $\tan\beta$ which determine the electroweakino couplings to Higgs and gauge bosons and therefore influence both the production cross section, in particular for Drell-Yan processes, and the dominant decay modes. As an example, the decay of $\chi_i^0 \to \chi_1^0 h$ is strongest when one of the neutralinos is gauginolike and the other one is Higgsino-like, while the decay $\chi_i^0 \to \chi_1^0 Z$ is determined only by the Higgsino components of the neutralinos; see Eq. (2.1).

The processes of interest for this study are

$$pp \to \chi_i^+ \chi_j^- \to l^+ l^- + \not{E}_{\mathrm{T}} \tag{3.1}$$

and

$$pp \to \chi_i^+ \chi_j^0 \to 3\ell + \not{E}_{\mathrm{T}}, \tag{3.2}$$

where $\not{E}_{\mathrm{T}}$ represents the missing transverse energy arising from the $\tilde{\chi}_1^0$ and neutrinos.

The above processes can occur via (a) direct decays $\chi_i^\pm \to \chi_1^0 W^\pm$ and $\chi_i^0 \to \chi_1^0 Z/h$ or (b) cascade decays of higher chargino and neutralino states. Depending on the mass gap between the $\chi_i^\pm \chi_i^0$ and $\chi_1^0$, the $W/Z/h$ bosons can be on or off shell.

Since our primary motivation in this section is to assess the LHC constraints on light neutralinos, we choose three discrete values for $M_1$ ($M_1 = 5, 40, 60$ GeV) in order to cover the range of relevant LSP masses. Note that the mass of the lightest neutralino is roughly determined by the value of $M_1$, with corrections due to the mixing of other electroweakino mass parameters, which can reach a few GeVs especially when $\mu$ is also small. We then perform a scan in the $\mu - M_2$ plane and determine the constraints from the dilepton/trilepton + missing transverse energy (MET) searches performed at the LHC in the 8 TeV run. To this end we use the recasted LHC 8 TeV results in publicly available analyses databases in the framework of MadAnalysis5 [90] and Checkmate [91]. We do not include the currently available 13 TeV results [92] since a faithful recast of the corresponding electroweakino searches is not yet publicly available; however, we will briefly discuss below the prospects of improving the collider limits with higher luminosity.

The first search of interest is the ATLAS search for direct production of chargino and neutralino in the 3 lepton + MET channel as documented in [93]. The search is optimized on several scenarios, including light slepton or light staus in the intermediate state; however, the $WZ/Wh$ mediated scenario is the only one of relevance here. The basic selection criteria for the signal region requires one pair of same flavor opposite sign leptons among the three selected leptons with a transverse momentum ($p_T$) threshold of 25 GeV. The $WZ$ mediated signal region has 20 disjointed bins based on the MET, the invariant mass of the same flavor opposite sign leptons and the transverse mass between the third lepton and MET. The other signal regions in this analysis follow a similar pattern. This analysis has been validated in the Checkmate framework, the details of which can be found in [91].

The second search of interest is the ATLAS search for direct production of charginos and neutralinos in the dilepton + MET final state [94]. The opposite sign dilepton + MET, via intermediate state $W$ signature arises from chargino pair production followed by the decay to the LSP and leptons bosons. Signal regions are divided into two criteria, first requiring a veto on the $Z$ boson and the second without. This analysis was recasted and validated in the public analysis database (PAD) framework of MadAnalysis5. The details of the recasted analysis, the validation procedure, and the recast code can be found in [95]. As before, the validation was found to be reliable, and hence we use this analysis to constrain the parameter space.

Finally we also consider monojet + MET searches. It is well known that these searches work well for compressed decay topologies. However, it has also been noted that it could probe light DM for certain classes of models [96]. Thus, we assess whether the constraints in regions where the decay of charginos and neutralinos via the off shell

$W/Z$ boson lead to soft leptons and jets could be improved by monojet searches. For this we use the publicly available recasts of the ATLAS 8 and 13 TeV monojet + MET searches [96,97] available in the PAD framework. The two ATLAS monojet + MET searches are similar in terms of the nature of selection cuts and implementation, the difference being the strength of the applied cuts when going from 8 to 13 TeV. The analysis relies on the emission of one hard jet at the initial state, which recoils against the MET. The ATLAS analysis for both 8 and 13 TeV is divided into signal regions of increasing leading jet transverse momentum and MET. The details of the validation are documented, and the implemented code is available in [98,99].

We reinterpret the above searches by generating 100,000 events for each point in the $\mu - M_2$ plane for three discrete values of $M_1$, with $\tan\beta$ fixed to 10, corresponding to the processes described in Eqs. (3.1) and (3.2) using MadGraph5 [100]. The rest of the spectrum (including the sleptons) is decoupled from this set. The events are then passed to PYTHIA6 [101] for showering and hadronization. Jets are reconstructed using FASTJET [102], with the reconstruction parameters chosen to satisfy the requirements of each of the above analyses. Detector simulation is performed using Delphes [103] with the detector parameters obtained from the validated cards for each of the above analysis. Cross sections for each point are calculated using Prospino [104]. Note that the cross section varies mildly with $\tan\beta$ and that this does not impact the collider bounds significantly. For each of the above recasts, the exclusion curves are obtained by built-in confidence level calculators following the $CL_s$ prescription [105]. In MadAnalysis5, for example, the module *exclusion-CLs.py* determines, given the number of signal, expected, and observed background events, together with the background uncertainty (the latter three directly taken from the experimental publications), the most sensitive signal region (SR) of the analysis and the exclusion C.L. using the $CL_s$ prescription for the most sensitive SR.

In Fig. 1, we present the 95% C.L. contours in the $\mu - M_2$ plane for three values of $M_1$. The green shaded region is allowed points subject to the constraints on the light Higgs mass, the flavor physics constraints, and the LEP limit on the light chargino mass, along with the Higgs signal strength correlations from the combined CMS + ATLAS analysis. The solid lines correspond to the constraints from the trilepton search, while the dotted lines correspond to the dilepton search. We observe that the trilepton search is more constraining than the dilepton search except in the region of large $M_2$. These observations are consistent with the results obtained in [106]. There are various channels that contribute to the exclusion curves in this figure.

For the region at large $M_2$ excluded by the dilepton search, the main contributing processes are $pp \to \chi^0_{2,3}\chi^0_1$ with the heavier neutralinos decaying into $Z\chi^0_1$. The

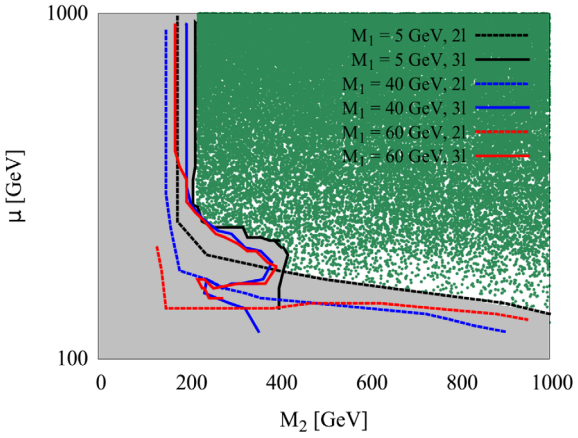


FIG. 1. The 95% C.L. contours in the $\mu - M_2$ plane from dilepton (dashed lines) and trilepton (solid lines) searches at LHC-8 TeV for $M_1 = 5, 40, 60$ GeV. Here $\tan\beta = 10$. Green points correspond to the allowed points of the scan after imposing all constraints in Sec. II. Only the region $\mu < 1$ TeV is displayed, as the contours are independent of $\mu$ for low values of $M_2$.

production cross sections decrease rapidly as $\mu$ increases and the LSP becomes pure bino, thus setting the exclusion. The dependence on $M_1$ is basically set by the detection efficiency as the BR of charginos/neutralinos into the LSP, and a gauge or Higgs boson is nearly 100% in all cases. As $M_2$ decreases, the process $pp \to \chi^+_1\chi^-_1$ contributes significantly to the exclusion, until for small values of $M_2$ when the chargino is dominantly wino it becomes the only relevant process. In this region, however, the best exclusions are set from the trilepton search. For the trilepton search, the majority of the exclusion originates from $pp \to \chi^+_1\chi^0_{2/3}$. At large values of $\mu$, $\chi^0_2$ is mostly wino and $pp \to \chi^+_1\chi^0_2$ is the dominant channel, the production cross section is determined by the value of $M_2$, and the exclusion contours are basically independent of $\mu$. For this reason, in Fig. 1, we show only the region up to $\mu = 1$ TeV. Note that in this region, the exclusion is more stringent for lower values of $M_1$. To a large extent this is due to more available missing energy, thus enhancing the efficiency of the search. For lower values of $\mu$ the production cross sections for both $\chi^+_1\chi^0_2$ and $\chi^+_1\chi^0_3$ increase, thus extending the reach, until some value of $M_2$ where the search loses sensitivity partly because of the low cross sections involved. Note that these limits are derived using the best expected signal region; however, the best signal region jumps in the region of parameter space near the curve excluded by the trilepton search, and hence the contour is uneven. Finally the monojet searches (from both 8 and 13 TeV) do not constrain the parameter space. The reason for this is twofold. Since the dark matter is light, the jet recoiling against this light object is not hard enough, and therefore the acceptance × efficiency is not large. As the production cross section is low, this inefficiency in acceptance is not compensated. We would like to mention here

that we have implemented the exclusion limits derived at 95% C.L. from the dilepton and trilepton searches from LHC 8 TeV data, which are shown in Fig. 1, on our parameter space of interest.

We performed a study based on the cuts designed to probe electroweakinos at the high luminosity LHC [107], for low to intermediate values of $\mu$ and $M_2$ (200–400 GeV), and observed that the selection cuts for the search were not optimal to probe this region of the parameter space. Thus, a detailed study for the high luminosity LHC run is required and will be the subject of a follow-up to this work. We emphasize that all the regions with charginos lighter than 500 GeV (roughly $\mu, M_2 < 500$ GeV) can easily be probed at a TeV scale ILC.

## IV. THE NEUTRALINO AS A THERMAL RELIC

In this section, we consider the case where the neutralino is a thermal relic and discuss the impact of DM observables including the relic density and the elastic scattering of DM with nucleons. Within the standard cosmological model, the neutralino relic density is computed using micrOMEGAs (version 4.2.3) [80–82] and compared with the very precise measurement done by the PLANCK Collaboration [108], $\Omega^{\rm obs}_{\rm DM}h^2 = 0.1184 \pm 0.0012$ at 68% C.L. Assuming a $3\sigma$ interval, we obtain a window of $\Omega^{\rm obs}_{\rm DM}h^2 = 0.1148$–$0.1220$, and adopting a conservative approach, we impose an upper limit, $\Omega_{\rm DM}h^2 \leq 0.1220$. Here we assume implicitly that either there is another DM component when the observed value is not saturated or the observed value is attained through nonthermal mechanisms. We also impose the constraints from LEP, flavor physics, and Higgs physics, listed in Sec. II and consider only the region where the Higgs decay into neutralinos is kinematically accessible.

Imposing the DM relic density bound sets a lower limit on the LSP mass, $M_{\tilde{\chi}^0_1} \gtrsim 34$ GeV. As mentioned previously, the LEP limits on charged particles entail that the neutralino DM, $\tilde{\chi}^0_1$, be bino-dominated with mixtures from Higgsino as well as wino. Within our framework, the only mechanisms for achieving efficient DM annihilation are the exchange of a $Z$ or a Higgs boson. As expected, we observe that allowed points are restricted to the funnel regions with the LSP mass near $m_Z/2$ or $m_h/2$. After taking into account the constraints from the Higgs signal strengths which effectively restrict the coupling of the LSP to the Higgs, in fact reducing the Higgsino component of the LSP and thus also its coupling to the $Z$, the mass of the LSP is forced to lie even closer to either resonance. The impact of the Higgs coupling constraints is displayed in Fig. 2(a) which shows the branching fraction of the $CP$-even light Higgs boson ($h$) to a pair of $\tilde{\chi}^0_1$ [$\mathrm{Br}(h \to \tilde{\chi}^0_1\tilde{\chi}^0_1)$] as a function of the LSP mass, $M_{\tilde{\chi}^0_1}$. The grey points satisfy only the Higgs mass constraint, the flavor physics constraints, and LEP limits mentioned in Sec. II, whereas the colored points also satisfy the constraints from Higgs signal strength measurements. We observe that after applying the latter, the Higgs to invisible branching fraction is restricted to $\lesssim$10%. A high invisible Higgs branching fraction severely affects its branching to the SM decay modes, resulting in the signal strength values receiving a strong shift from their SM values and, as a result, falling outside the 95% C.L. Higgs signal strength correlation contours discussed in Sec. II. We show the direct ILC reach in the Higgs to invisible mode

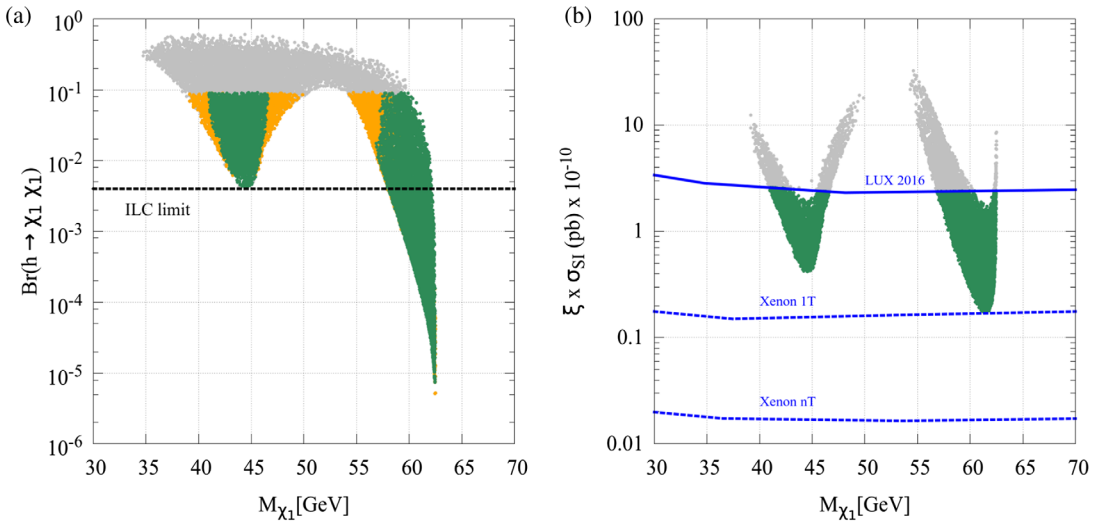


FIG. 2. (a) The Higgs to invisible branching $\mathrm{Br}(h \to \tilde{\chi}^0_1\tilde{\chi}^0_1)$ vs the LSP mass $M_{\tilde{\chi}^0_1}$. The grey (colored) points distinguish the points allowed before (after) the Higgs signal strength constraints. Yellow (green) points are excluded (allowed) by the current limits on the SI WIMP-nucleon cross section from LUX-2016 [109]. The black-dashed line represents the ILC reach, $\mathrm{Br}(h \to \tilde{\chi}^0_1\tilde{\chi}^0_1) > 0.4\%$ [25]. (b) SI WIMP-nucleon cross section vs $M_{\tilde{\chi}^0_1}$ for all points allowed by collider and relic density constraints. The blue-solid line shows the current limit from LUX-2016 [109], and the blue-dashed lines show the projected reach for Xenon-1T [110] and Xenon-nT [110].

[$\mathrm{Br}(h \to \mathrm{invi}) > 0.4\%$ [25]] through a black dashed line in Fig. 2(a). It can be observed from Fig. 2(a) that the ILC will be able to probe the entire $Z$ funnel region through the Higgs to invisible branching. However, in the Higgs resonance region, the Higgs to invisible branching fraction attains a value as low as $\approx 10^{-5}$; thus a significant fraction of points will evade detection by ILC (through the Higgs to invisible decay mode). The reason for the small invisible width is, on the one hand, the small LSP-Higgs coupling and, on the other hand, phase space suppression. Finally, note that the points for which the relic density falls precisely within the observed range lie at the lower edge of the colored region in Fig. 2(a).

In recent years, DM direct detection experiments which exploit spin-independent (SI) or spin-dependent (SD) weakly interacting massive particle (WIMP)-nucleon elastic scattering have provided very sensitive probes of DM. Since the SI WIMP-nucleon experiments are more sensitive than their SD counterpart, in our framework, we display only the predictions and the limits from SI WIMP-nucleon interaction in Fig. 2(b). Here, the grey and green colored parameter space points satisfy all the constraints mentioned in Sec. II; however, the grey points are excluded by the current LUX limits [109]. Typically the excluded points are those with a larger Higgsino component as the elastic scattering cross section is dominated by the Higgs exchange, and hence depends directly on the LSP-Higgs coupling. Note that the LUX-2016 limit permits the exclusion of many points for which the invisible Higgs width is small (even only 1%) and is therefore more stringent than current Higgs precision measurements; see Fig. 2(a). Moreover, the upcoming Xenon-1T experiment [110] will be able to probe the entire allowed parameter space, as is evident from Fig. 2(b). The exclusion limits are obtained assuming a local density of DM $\rho = 0.3\ \mathrm{GeV/cm^3}$, large uncertainties in its determination can introduce a large shift in the limit extracted [111], and the conventional value used leads to a somewhat conservative limit.

Note that we have rescaled the SI WIMP-nucleon cross section ($\sigma_{\mathrm{SI}}$) with $\xi$, defined as the ratio of predicted DM relic density $\Omega h^2$ to the observed one $\Omega_{\mathrm{DM}} h^2$ (0.122, allowing a $3\sigma$ interval around the best-fit value derived by PLANCK Collaboration [108]),

$$\xi = \frac{\Omega}{\Omega_{\mathrm{DM}}} = \frac{\Omega}{0.122}. \tag{4.1}$$

The predictions for the rescaled spin dependent cross section on protons ($\sigma_{\mathrm{SD}}^{\mathrm{proton}}$) and on neutrons ($\sigma_{\mathrm{SD}}^{\mathrm{neutron}}$) are shown in Fig. 3 together with the current limits from LUX [112] and the future projections from PICO-250 [113] for $\sigma_{\mathrm{SD}}^{\mathrm{proton}}$ and from LZ [112] for $\sigma_{\mathrm{SD}}^{\mathrm{neutron}}$. Note that the cross sections on protons and neutrons are very similar. PICO-250 and LZ will be able to probe the entire $Z$ resonance region, while part of the Higgs resonance region remains out of reach of planned detectors.

We show the variation of $\xi$ with the LSP mass in Fig. 4(a). Finally, we comment on the prospects to probe the allowed parameter space at the ILC, in particular through chargino searches. In this channel, all kinematically accessible chargino pairs can be probed. To be conservative and for simplicity, we define the ILC-1 TeV reach as $\mu$ or $M2 < 500$ GeV, following [114]. In Fig. 4(b), we display all parameter points allowed by collider, relic density, and LUX-2016 constraints in the $\mu - M_{\tilde{\chi}_1^0}$ plane. We distinguish four possible scenarios after considering the following two possible modes of DM probe by ILC:

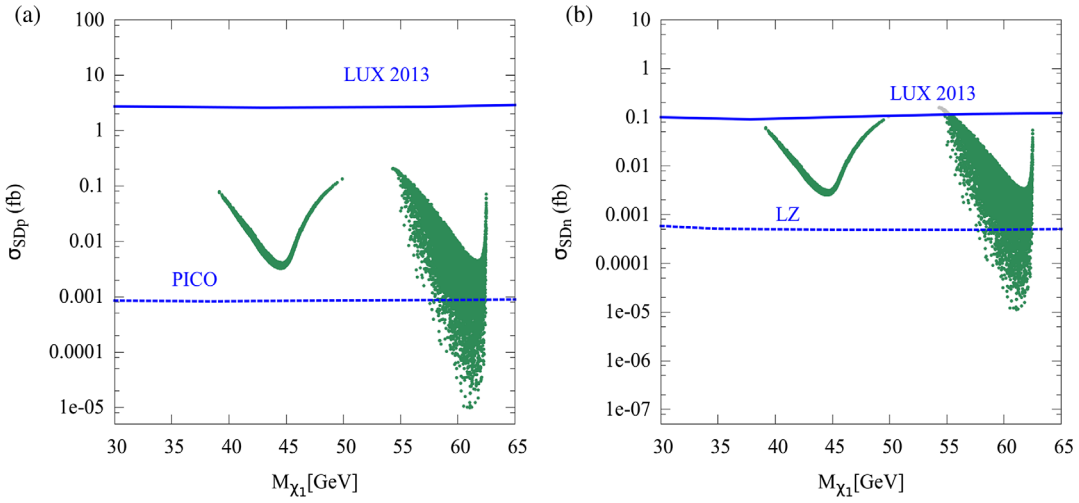


FIG. 3. (a) SD WIMP-proton cross section vs $M_{\tilde{\chi}_1^0}$ for all points allowed by collider and relic density constraints. The blue-solid line shows the current limit from LUX-2013 [112], and the blue-dashed line shows the projected reach for PICO-250 [113]. (b) SD WIMP-neutron cross section vs $M_{\tilde{\chi}_1^0}$ for all points allowed by collider and relic density constraints. The blue-solid line shows the current limit from LUX-2013 [112], and the blue-dashed line shows the projected reach for LZ [112].

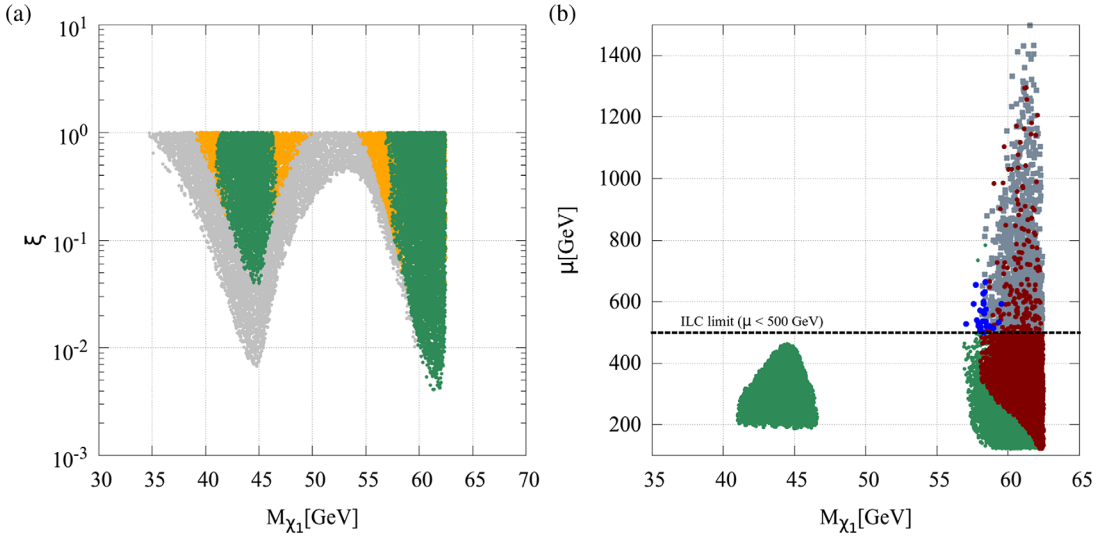


FIG. 4. (a) The normalized relic density, $\xi = \Omega_{\rm DM}/0.122$, vs the LSP mass, using the same color code as in Fig. 2(a). (b) Higgsino mass parameter $\mu$ against the LSP mass, where the black dashed line represents the ILC sensitivity to probe $\mu < 500$ GeV. Here, only the parameter points allowed by collider constraints and LUX-2016 have been considered. The color code is described in the text.

(1) *Mode A*: through Higgs to invisible branching, $\mathrm{Br}(h \to \tilde{\chi}_1^0\tilde{\chi}_1^0) > 0.4\%$.
(2) *Mode B*: through electroweakino searches: $\mu, M_2 < 500$ GeV.
   (a) *Probe via mode A and mode B*: These points are shown in green and have $\mathrm{Br}(h \to \tilde{\chi}_1^0\tilde{\chi}_1^0) > 0.4\%$ as well as $\mu$ or $M_2 < 500$ GeV.
   (b) *Probe via mode A only*: These points, in blue, have $\mathrm{Br}(h \to \tilde{\chi}_1^0\tilde{\chi}_1^0) > 0.4\%$ as well as $\mu, M_2 > 500$ GeV.
   (c) *Probe via mode B only*: These points, in brown correspond to $\mathrm{Br}(h \to \tilde{\chi}_1^0\tilde{\chi}_1^0) < 0.4\%$ and $\mu$ or $M_2 < 500$ GeV.
   (d) *Cannot be probed by ILC:* These points are shown in grey.

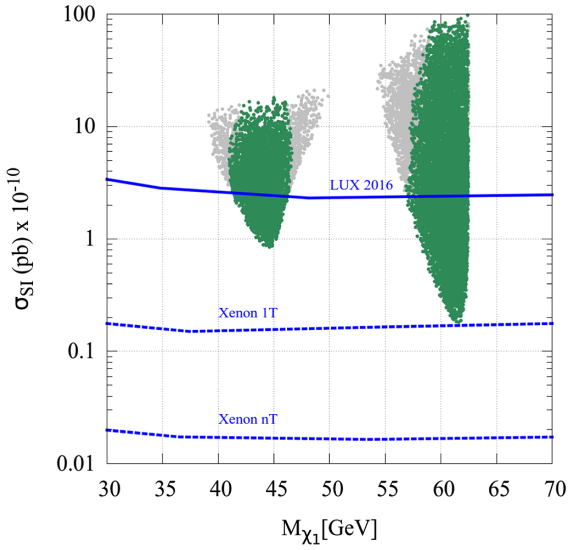


FIG. 5. Unscaled SI WIMP-nucleon cross section vs $M_{\tilde{\chi}_1^0}$ for all points allowed by collider and relic density constraints. The blue-solid line shows the current limit from LUX-2016 [109], and the blue-dashed lines show the projected reach for Xenon-1T [110] and Xenon-nT [110].

The ILC can therefore completely probe the $Z$-funnel region, just as would be possible with DM direct detection with Xenon-1T, while a fraction of the Higgs funnel remains out of reach. We find only a limited number of points that can be exclusively probed through the Higgs invisible width.

Before concluding this section we comment on the implications of allowing for a nonthermal mechanism to increase the value of the relic density to the observed value. This entails that the neutralino would constitute all of the DM; thus there is no need to rescale the elastic scattering cross-sections on nucleons. In Fig. 5, we show the unscaled $\sigma_{\rm SI}$ against $M_{\tilde{\chi}_1^0}$, with the green and grey colored points being the same as that of Fig. 2(b). As expected, the constraint from LUX is now more stringent, and a significant number of parameter space points are now excluded. This effect is more prominent in the $Z$-resonance region, where we observe an upward shift in the funnel region, and a factor of 3 improvement over the current LUX limits would suffice to exclude this region. In the next section, we further relax the assumption of a thermal relic and explore the parameter space specified in Sec. II, in the context of limits from ILC and DM direct detection experiments, following a similar approach to the one adopted in this section.

## V. PROBING OVERABUNDANT NEUTRALINOS

Assuming a thermal production of DM, we have seen that the relic density provides strong constraints on the

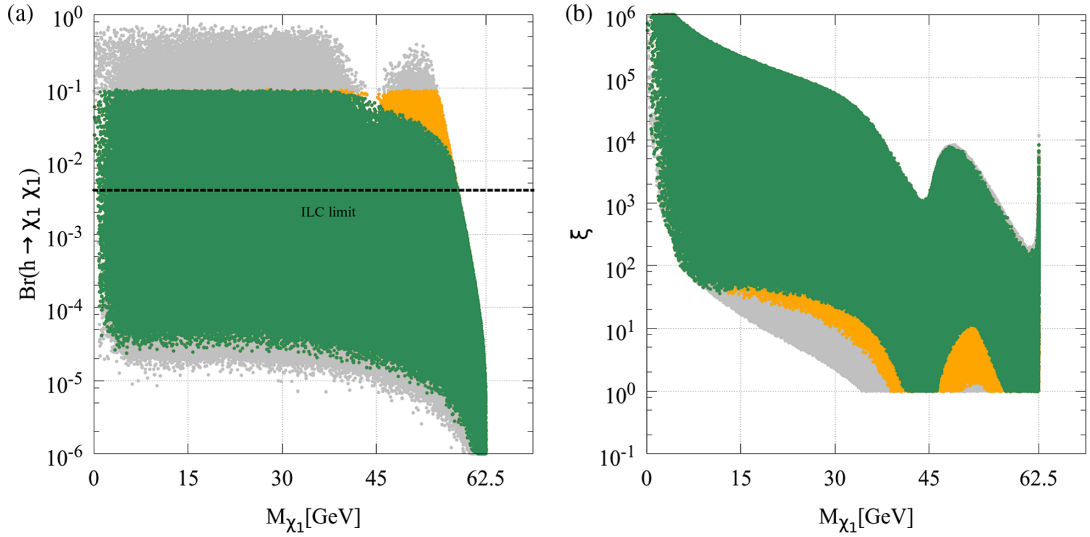


FIG. 6. (a) The Higgs to invisible branching fraction $\mathrm{Br}(h \to \tilde{\chi}_1^0 \tilde{\chi}_1^0)$ vs the LSP mass $M_{\tilde{\chi}_1^0}$. (b) The rescaled relic density, $\xi$, against $M_{\tilde{\chi}_1^0}$. Same color code as Fig. 2.

MSSM parameter space. In particular, binolike neutralinos lighter than roughly 34 GeV are ruled out as their annihilation cross section is too small, leading to a predicted value for the relic density ($\Omega_{\mathrm{CDM}}$) that can be orders of magnitude larger than the observed value ($\Omega_{\mathrm{DM}}$). However, there is ample motivation for considering nonthermal mechanisms that lead to much different predictions and that allow one to reproduce the observed value of the DM relic density. The prime example is the case of a late decaying particle, such as a SUSY modulus scalar, where the late decaying particle dilutes the entropy density and can thus lead to the correct value for the relic density of DM ($\Omega_{\tilde{\chi}_1^0}$). The amount of dilution is sensitive to the mass of the heavy decaying particle ($m_\phi$). The dilution also depends on the mass of the DM, the branching ratio of the heavy particle to DM, and the reheating temperature. Hence, for every value of DM mass, several combinations of reheating temperature and heavy scalar mass can lead to a relic density compatible with the observed value,

$$\frac{\Omega_{\tilde{\chi}_1^0}}{\Omega_{\mathrm{DM}}} \propto b n_\phi m_\chi T_{\mathrm{RH}}, \tag{5.1}$$

where $b$ is the number of neutralinos produced per $\phi$ decay, $n_\phi$ the number density of the scalar, and $T_{\mathrm{RH}}$ the reheating temperature [69,115]. Here, we will not perform a detailed investigation of a specific nonthermal mechanism but will simply assume that it is possible to find a mechanism that brings the DM relic density in agreement with observations. Hence, in practice we will analyze all those parameter space points, for which the relic density values computed assuming thermal freeze-out with a standard cosmological model, is above the measured value,

$$\Omega_{\tilde{\chi}_1^0} h^2 > 0.122, \tag{5.2}$$

and we will investigate the characteristics and the signatures of the thermally overabundant neutralino, hereafter called NSDM neutralino.

With this condition, the lower bound on the lightest neutralino mass is lifted, and we obtain LSPs with masses that span the whole range of the scan (up to 62.5 GeV). The resulting Higgs to invisible branching fraction [$\mathrm{Br}(h \to \tilde{\chi}_1^0 \tilde{\chi}_1^0)$], for all points that satisfy all the constraints mentioned in Sec. II, have been shown in color in Fig. 6(a). The grey points in the same figure are excluded by the Higgs signal strength constraints. As in the previous section, we observe that imposition of the Higgs signal strength constraints translate into an upper bound on the Higgs to invisible branching fraction, which is again approximately ≈10%. In addition, we observe that some parameter space points with a very small Higgs to invisible branching fraction, $\mathrm{Br}(h \to \tilde{\chi}_1^0 \tilde{\chi}_1^0) \lesssim 10^{-6}$, are also disallowed by the Higgs signal strength constraints. For these points, the partial decay width of $h \to b\bar{b}$ attains a value which is appreciably greater than the SM expectations, leading to significant deviations from the SM, in the branching of $h \to ZZ$ and $h \to WW$ (and consequently $h \to \gamma\gamma$). We find that allowing for nonstandard cosmology, the Higgs to invisible branching fraction can vary over a wide range and can attain values as low as $\mathrm{Br}(h \to \tilde{\chi}_1^0 \tilde{\chi}_1^0) \sim 10^{-6}$ in the Higgs resonance region. It can be observed from Fig. 6(a) that very small values of $\mathrm{Br}(h \to \tilde{\chi}_1^0 \tilde{\chi}_1^0)$ can be obtained for very light DM, which is a direct consequence of relaxing the relic density constraint, since an efficient annihilation mechanism is no longer required, and thus, the coupling of the LSP to the Higgs can be very small. The yellow points in Fig. 6(a) are excluded by the current limits

on SI WIMP-nucleon interaction cross sections from LUX-2016 [109]. Typically, these yellow colored points correspond to a large LSP-Higgs coupling, resulting in a large invisible width, and hence exclude the region with $M_{\tilde{\chi}_1^0} \gtrsim 15$ GeV, where direct detection has a better sensitivity. The green colored parameter space points are still allowed by all colliders and direct detection limits and will be referred to as the allowed parameter space in the remainder of this section. Assuming a standard thermal DM scenario, we obtain values of the relic density, illustrated by $\xi$ in Fig. 6(b). It can be seen that the value of $\xi$ for the allowed parameter space is at least around 2 orders of magnitude above the observed limits for all $M_{\tilde{\chi}_1^0} \lesssim$ 30 GeV and reach the limit of validity of the micrOMEGAs computation for $M_{\tilde{\chi}_1^0} \lesssim 10$ GeV ($\xi \sim 10^6$).

The prospects for direct detection are illustrated in Fig. 7, where we show the limits on SI WIMP-nucleon cross section from LUX-2016 [109] and the reach of Xenon-1T [110] and Xenon-nT [110]. In contrast to the thermal DM case, a significant fraction of the points are below the reach of Xenon-1T and even the future Xenon-nT. Clearly many points are below the threshold for detection but there are also points with $M_{\tilde{\chi}_1^0} > 30$ GeV which will be undetectable at the large-scale detectors, where the direct detection (DD) experiments have an excellent sensitivity. Moreover, the SI cross section at low mass is predicted to lie below the coherent neutrino background. Thus even future experiments such as SuperCDMS-SNOLAB [116] designed to enhance the sensitivity at low masses will not be able to probe this region.

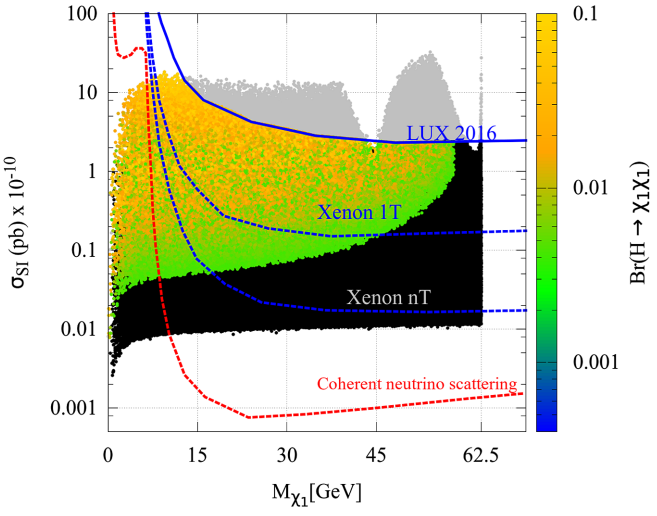


FIG. 7. SI WIMP-nucleon cross section vs $M_{\tilde{\chi}_1^0}$ for all points allowed by collider and relic density constraints. The color code characterizes the value of $\mathrm{Br}(h \to \tilde{\chi}_1^0\tilde{\chi}_1^0)$, while black points have $\mathrm{Br}(h \to \tilde{\chi}_1^0\tilde{\chi}_1^0) < 0.4\%$. The blue-solid line shows the current limit from LUX-2016 [109], and the blue-dashed line shows the reach for Xenon-1T [110] and Xenon- nT [110].

To draw a better illustration of the complementarity between the Higgs invisible branching and the DD cross sections, we color coded the allowed points in Fig. 7 according to the Higgs invisible branching fraction. Points with $\mathrm{Br}(h \to \tilde{\chi}_1^0\tilde{\chi}_1^0) \lesssim 0.4\%$ have been shown in black, while an overlapping color palette has been used for those parameter space points which can be probed at ILC through the Higgs to invisible branching fraction. Interestingly, a large fraction of the points that are below the threshold for direct detection are within the reach of the ILC, while a fraction of points can be probed both at the ILC and with ton scale DD detectors. There also exists such points which are out of reach of both the detection methods. We present the parameter space points which satisfy all the constraints of Sec. II in the $\sigma_{SD}^{\tilde{\chi}_1^0\mathrm{prot}}$-$M_{\tilde{\chi}_1^0}$ ($\sigma_{SD}^{\tilde{\chi}_1^0\mathrm{neut}}$-$M_{\tilde{\chi}_1^0}$) plane as well, in Fig. 8(a) [Fig. 8(b)]. It can be observed that the current limits from LUX-2013 are not strong enough to exclude the parameter space points except for a few at $M_{\tilde{\chi}_1^0} \approx 55$ GeV, which are excluded by the SD WIMP-neutron cross-section limits, as evident from Fig. 8(b).

We present the allowed parameter space in the $M_{\tilde{\chi}_1^\pm} - M_{\tilde{\chi}_1^0}$ plane in Fig. 9 in order to investigate the implications of ILC sensitivity to probe $\mu, M_2 < 500$ GeV through electroweakino searches. $\mu = 500$ GeV has been shown as a black-dashed line in Fig. 9. Similar to the previous section, the parameter space points in Fig. 9 have been classified into following four different categories based on the two different detection modes of ILC,

(1) *Mode A*: through Higgs to invisible branching, $\mathrm{Br}(h \to \tilde{\chi}_1^0\tilde{\chi}_1^0) > 0.4\%$.
(2) *Mode B*: through electroweakino searches, $\mu, M_2 < 500$ GeV.
   (a) *Probed by ILC through mode A* and mode *B*: These points have been represented in green in Fig. 9. These parameter space points have $\mathrm{Br}(h \to \tilde{\chi}_1^0\tilde{\chi}_1^0) > 0.4\%$ as well as either $\mu <$ 500 GeV and/or $M_2 < 500$ GeV.
   (b) *Probed by ILC only through mode A*: These parameter points have been represented in brown. Both $\mu$ and $M_2$ are above 500 GeV for these points, and $\mathrm{Br}(h \to \tilde{\chi}_1^0\tilde{\chi}_1^0) > 0.4\%$.
   (iii) *Probed by ILC through mode B*: We show these parameter space points in yellow. These parameter points have $\mu < 500$ GeV and/or $M_2 < 500$ GeV, along with $\mathrm{Br}(h \to \tilde{\chi}_1^0\tilde{\chi}_1^0) \leq 0.4\%$.
   (iv) *Points which cannot be probed by ILC*: These parameter space points have been shown in grey. For these parameter space points, $\mathrm{Br}(h \to \tilde{\chi}_1^0\tilde{\chi}_1^0) < 0.4\%$, $M_2 < 500$ GeV, and $\mu < 500$ GeV. Hence, these parameter points evade detection by ILC.

It can be observed from Fig. 9 that ILC will be capable of probing a significant fraction of the allowed parameter space considering ILC's detection capability through both

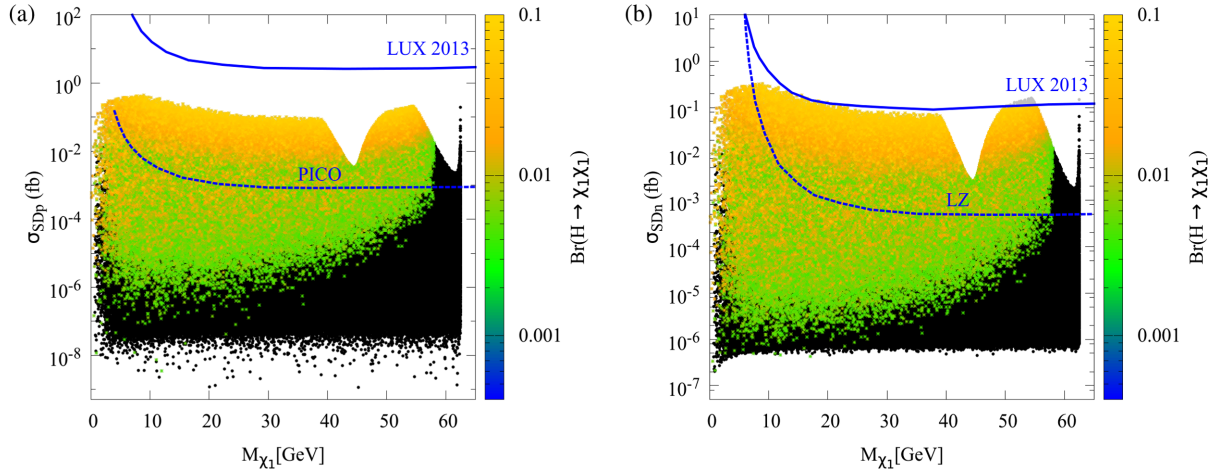


FIG. 8. (a) SD WIMP-proton cross section vs $M_{\tilde{\chi}_1^0}$ for all points allowed by collider and relic density constraints. The blue-solid and blue-dashed lines show the current limits from LUX-2013 [112] and the reach of PICO-250 [113], respectively. (b) SD WIMP-neutron cross section vs $M_{\tilde{\chi}_1^0}$ for all points allowed by collider and relic density constraints. The blue-solid line and the blue-dashed line show the current limits from LUX-2013 [112] and the reach of LZ [112], respectively. The color code characterizes the value of $\mathrm{Br}(h \to \tilde{\chi}_1^0\tilde{\chi}_1^0)$, and black points have $\mathrm{Br}(h \to \tilde{\chi}_1^0\tilde{\chi}_1^0) < 0.4\%$.

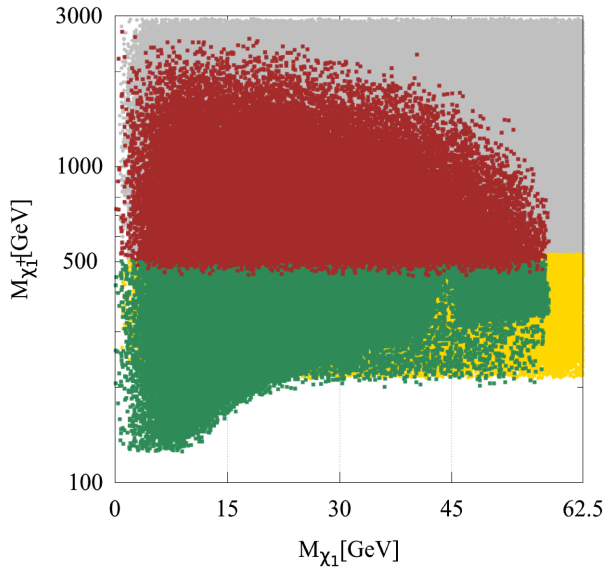


FIG. 9. Represents the chargino mass ($M_{\tilde{\chi}_1^\pm}$) against $M_{\tilde{\chi}_1^0}$ for the allowed parameter space points. The corresponding color code is mentioned in the text.

mode A and mode B. However, a notable fraction of parameter space points will evade detection by ILC as well as from the current DM direct detection experiments, as evident from the grey colored points in Fig. 9.

## VI. COMPLEMENTARITY OF FUTURE EXPERIMENTS IN PROBING DARK MATTER

In this section we characterize the different possibilities to identify the nature of dark matter by exploiting the complementarity between the ILC, through a precise measurement of the Higgs invisible width or the detection of electroweakinos, and future SI or SD direct detection experiments. Here we mean the detectors beyond the ones currently in operation, more specifically XENON-nT (through SI WIMP-nucleon based interaction), PICO-250 (through SD WIMP-proton based interaction), and LZ (through SD WIMP-neutron based interaction). For the sake of simplifying the discussion, we adopt the simple criteria that the limit of detectability for electroweakinos at the ILC is $\mu < 500$ GeV.[1] In addition to detecting new particles, the ILC will also be capable of performing very precise electroweakino mass measurements with an uncertainty of less than 1 GeV [117] and thus will allow one to determine the gaugino masses and the value of $\mu$. Moreover, we note that the LSP mass can be determined in direct detection experiments albeit with a large uncertainty. This also requires that a certain number of events are observed [118]. For example, the mass of a WIMP of ∼50 GeV can be measured to ∼35% with 100 events. To organize the discussion, in the following subsections we group the points according to the type of experiment that has the potential to probe them. For this we consider all scenarios that satisfy current collider and flavor constraints regardless of whether thermal dark matter can reproduce the observed relic density and point out the conditions for distinguishing thermal and NSDM scenarios.

[1]The ILC can also just as easily probe values of $M_2 < 500$ GeV; however, the nearly pure winos would first be discovered at the LHC.

### A. Detection at the ILC only

The first class of scenarios we consider are those that can be probed exclusively through the Higgs to invisible branching fraction at ILC. These parameter points will evade detection at all the future DD experiments (Xenon-nT, PICO-250, and LZ) considered in this analysis. We show the parameter points with $\mathrm{Br}(h \to \tilde{\chi}_1^0\tilde{\chi}_1^0) > 0.4\%$ in the $\mathrm{Br}(h \to \tilde{\chi}_1^0\tilde{\chi}_1^0) - M_{\tilde{\chi}_1^0}$ plane in Fig. 10. The color palette corresponds to the value of $\mu$.

As expected, the points are concentrated in the low mass region, $M_{\tilde{\chi}_1^0} \lesssim 18$ GeV, corresponding to DM masses mostly inaccessible to direct detection. In this case, the branching fraction of $h \to \tilde{\chi}_1^0\tilde{\chi}_1^0$ goes up to $\approx$10% for relatively low values of $\mu$ as shown in the color palette in Fig. 10. Note that the points with $M_{\tilde{\chi}_1^0} > 12$ GeV are associated with a larger value of $\mu$, thus are more weakly coupled to the Higgs, and evade direct detection limits despite being above the threshold.

In Fig. 11, we show the same parameter space points in the $\xi - M_{\tilde{\chi}_1^0}$ plane with the color palette representing the value of $\mu$. All the points have $\xi > 500$ with the higher values attained at low $\tilde{\chi}_1^0$ masses. It can be concluded from Fig. 11 that observation of a DM signal exclusively through the Higgs to invisible branching fraction would be a strong indication for the DM candidate to be light and an artifact of nonstandard cosmology.

A subclass of the scenarios that can be probed through the invisible decay of Higgs boson at the ILC feature $\mu \leq 500$ GeV, and are thus accessible through electroweakino searches at ILC. We observe that such scenarios are restricted to $M_{\tilde{\chi}_1^0} \lesssim 12$ GeV and that a combined determination of the LSP mass and of $\mu$ at the ILC would clearly point toward nonthermal scenarios since $\xi \sim [2500:5000]$.

A similar conclusion can be reached for another subclass of scenarios which evade future DD limits and are detectable exclusively at ILC through the electroweakino searches. These scenarios feature a smaller value of $M_1$,

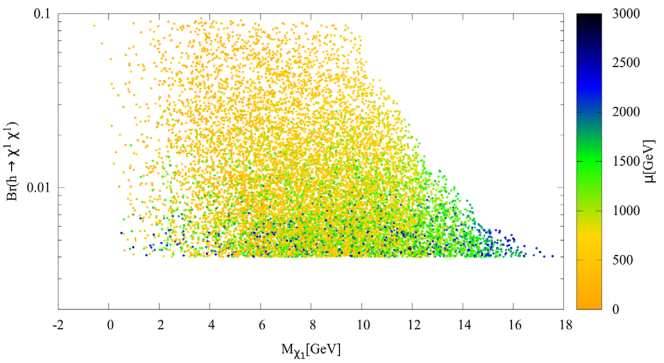


FIG. 10. Scatter plot in the $\mathrm{Br}(h \to \tilde{\chi}_1^0\tilde{\chi}_1^0) - M_{\tilde{\chi}_1^0}$ plane for parameter space points which can be probed by ILC only, through the Higgs to invisible branching fraction. The color palette corresponds to the value of the Higgsino mass parameter ($\mu$).

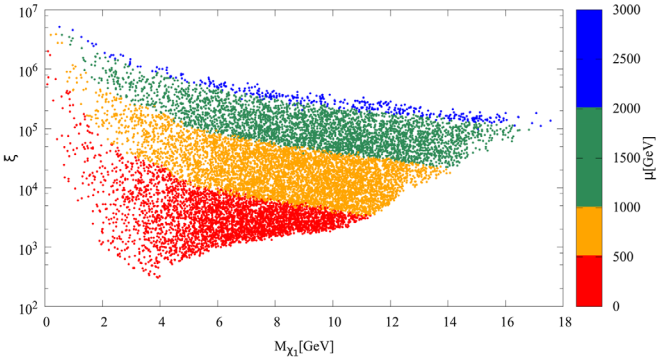


FIG. 11. Scatter plot in the $\xi - M_{\tilde{\chi}_1^0}$ plane for parameter space points which can be probed by ILC only, through the Higgs to invisible branching fraction [$\mathrm{Br}(H \to \tilde{\chi}_1^0\tilde{\chi}_1^0) \geq 0.4\%$]. The color palette corresponds to the value of the Higgsino mass parameter ($\mu$).

leading to $M_{\tilde{\chi}_1^0} \lesssim 10$ GeV, are nearly pure bino, and thus are associated with $\mathrm{Br}(H \to \tilde{\chi}_1^0\tilde{\chi}_1^0) \leq 0.4\%$ even though the Higgsino parameter is small, $\mu \leq 500$ GeV. The precise mass determination capability of the ILC will thus allow one to clearly identify NSDM scenarios, since in this case $\xi$ is found to be $10^3$–$10^4$ for $M_{\tilde{\chi}_1^0} > 5$ GeV. Note that for the scenarios described in this subsection we have also checked the impact of a precise measurement of the Higgs total width at the ILC and found that it did not provide any additional constraints on the parameter space.

### B. Detection at Xenon-nT only

In this subsection, we examine those parameter space points which can be probed by the Xenon-nT detector only, through the SI WIMP-nucleon interaction cross sections. These parameter space points evade detection by other future DD experiments, such as PICO-250 and LZ, as well as from ILC through Higgs to invisible branching fraction since $\mathrm{Br}(h \to \tilde{\chi}_1^0\tilde{\chi}_1^0) \leq 0.4\%$. We show these parameter space points in Fig. 12 in the $\xi - M_{\tilde{\chi}_1^0}$ plane with $\mu$ represented as a color palette.

Within this scenario, $\xi$ varies from $\sim 10^{-3}$ all the way up to $\sim 5 \times 10^4$ with a spread over 7 orders of magnitude. We obtain parameter space points with a relic density $\Omega_{\mathrm{DM}}h^2 < 0.122$, representing a relic from standard cosmological history, only in the Higgs resonance region. It is, however, difficult not only to know precisely enough the LSP mass to establish that it lies within the Higgs resonance region but also to identify whether the signature corresponds to a relic from standard or nonstandard cosmology.

However, there are unique scenarios, where it becomes possible to obtain more precise information about the relic density of $\tilde{\chi}_1^0$, based on specific categorization of $\mu$ and $M_{\tilde{\chi}_1^0}$. For example, we encounter some parameter space points with $\mu < 500$ GeV, making them accessible to ILC through the electroweakino searches. These parameter

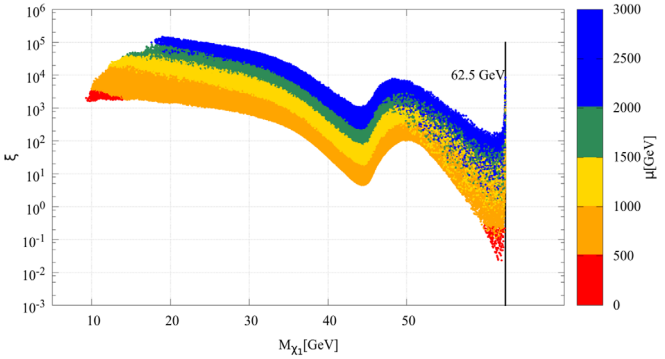


FIG. 12. Scatter plot in the $\xi - M_{\tilde{\chi}_1^0}$ plane for parameter space points which can be probed by Xenon-nT only, through the SI WIMP-nucleon interactions. The color palette corresponds to the value of the Higgsino mass parameter ($\mu$).

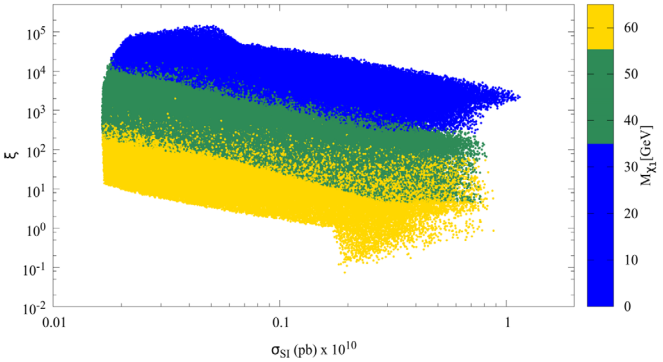


FIG. 13. Scatter plot in the $\xi - M_{\tilde{\chi}_1^0}$ plane for parameter space points which can be probed by Xenon-nT only, through the SD WIMP-nucleon interactions. For these parameter space points $\mu > 500$ GeV. The color palette corresponds to the value of $M_{\tilde{\chi}_1^0}$.

points (shown in red in Fig. 12) are restricted to two well separated and compact regions: (a) $M_{\tilde{\chi}_1^0} \sim 9$–$15$ GeV with $\xi$ within the range 2500–3000, and (b) $M_{\tilde{\chi}_1^0} \sim 57$–$62.5$ GeV with $\xi$ within the range 0.01–0.5. Taking into account ILC's capability to precisely measure the mass of the neutralino, it can be concluded that

(i) observation of a signal at Xenon-nT (through SI WIMP-nucleon interaction) and at the ILC (through electroweakino searches only) with a LSP compatible with the Higgs resonance region would indicate that the DM candidate ($\tilde{\chi}_1^0$) could be a relic from standard thermal history.

(ii) a similar observation, however, at low $M_{\tilde{\chi}_1^0} \sim 9$–$15$ GeV, would clearly indicate that the DM candidate is a relic of nonstandard cosmology.

DM mass measurements carried out by the DD based experiments, even if plagued by a large uncertainty will still be an useful tool for making better predictions for $\xi$. In Fig. 13, we show those parameter points of Fig. 12 which have $\mu > 500$ GeV, in the $\sigma_{\rm SI} - \xi$ plane with $M_{\tilde{\chi}_1^0}$ represented through the color palette. The ILC will be blind to these points in the electroweakino searches. In Fig. 13, we divide the parameter space into three different regions based on $M_{\tilde{\chi}_1^0}$. The nonresonant region ($M_{\tilde{\chi}_1^0} = 0$–$35$ GeV) is in blue, the $Z$-resonance region ($M_{\tilde{\chi}_1^0} = 35$–$55$ GeV) is in green, and the Higgs resonant region ($M_{\tilde{\chi}_1^0} > 55$ GeV) is in yellow. In summary, the Xenon-nT detector offers the best sensitivity for $M_{\rm DM} \gtrsim 20$ GeV. For these parameter space points, $\xi$ ranges from $\sim 10^{-2}$ to $\sim 5 \times 10^5$ with the highest value attained at low $M_{\rm DM}$ and the lowest value attained in the Higgs resonance region. In addition, there exists a small subgroup of parameter space points with $\mu < 500$ GeV which will be sensitive to the electroweakino searches at ILC. We found two such regions at very different mass ranges, one for $M_{\rm DM} \sim 9$–$15$ GeV with NSDM and the other for $M_{\rm DM} \sim 57$–$62.5$ GeV where thermal DM is underabundant. With the ILC's precise determination of the mass of $\tilde{\chi}_1^0$, an observation under this particular scenario will directly reveal whether the DM candidate is a thermal relic or an outcome of nonstandard cosmology. For parameter points with $\mu > 500$ GeV, the DD experiments can be employed for the determination of the DM masses. Although these mass measurements will have a significant error, they can be useful in inferring the thermal or nonthermal nature of DM, as shown in Fig. 13.

### C. Detection at Xenon-nT and at the ILC with invisible Higgs

Here we analyze those parameter space points which would be visible at ILC through the Higgs to invisible branching fraction and in some cases through electroweakino searches as well and also accessible at Xenon-nT through SI based interactions. Other DD experiments considered in this analysis would be blind to these parameter space points. We display these parameter space points in Fig. 14, in the $\xi - M_{\tilde{\chi}_1^0}$ plane along with $\mu$, shown through a color palette.

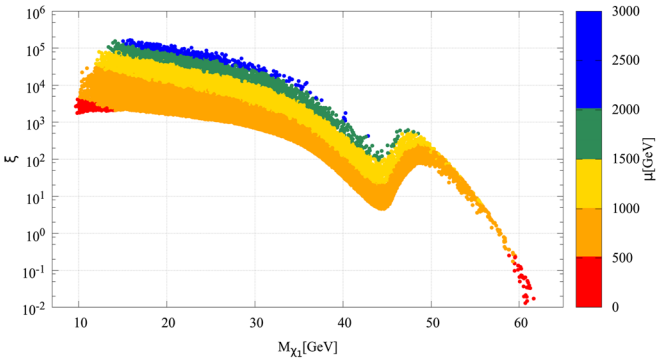


FIG. 14. Scatter plot in the $\xi - M_{\tilde{\chi}_1^0}$ plane for parameter space points which can be probed by Xenon-nT through the SI WIMP-nucleon interactions and also by ILC through the Higgs to invisible branching. The color palette corresponds to the value of the Higgsino mass parameter ($\mu$).

Parameter space points which fall under the purview of this scenario have similar characteristics to those described in the previous section. They extend over the mass range $M_{\tilde{\chi}_1^0} \sim 10$–$62$ GeV and are associated with either thermal or NSDM scenarios. The only difference with the scenario in Sec. VI B is that the LSP must couple sufficiently to the Higgs and therefore if close enough to $m_h/2$ will lead to $\xi \leq 1$. As above, we observe some parameter space points with $\mu \leq 500$ GeV that could be detected through the electroweakino searches at ILC (shown in red in Fig. 14). Those are confined within two separate regions of $M_{\tilde{\chi}_1^0}$, the first with $M_{\tilde{\chi}_1^0} \lesssim 15$ GeV and $\xi > 1000$, the second with $M_{\tilde{\chi}_1^0} \gtrsim 58$ GeV and $\xi$ within the range ∼0.05–0.5. With the possibility of a precise measurement of $M_{\tilde{\chi}_1^0}$, the following conclusions can be drawn:

(i) Observation of a signature at Xenon-nT through the SI WIMP-nucleon based interactions and also at ILC through both the Higgs to invisible branching fraction and electroweakino searches would indicate that the $\tilde{\chi}_1^0$ could be a standard thermal relic, provided $M_{\tilde{\chi}_1^0} \gtrsim 58$ GeV.

(ii) A similar observation, however, at low $M_{\tilde{\chi}_1^0} \lesssim 15$ GeV, would be an indicator of the DM candidate being a relic from nonstandard cosmology.

### D. Detection with PICO-250, the ILC, and/or Xenon-nT

In this subsection, we first analyze those parameter space points which can be probed by ILC through the Higgs to invisible branching, by PICO-250 through the SD WIMP-proton based interactions, and also by Xenon-nT through the SI WIMP-nucleon based interactions. These parameter space points are shown in Figs. 15(a) and 15(b), in the $\mathrm{Br}(h \to \tilde{\chi}_1^0\tilde{\chi}_1^0) - M_{\tilde{\chi}_1^0}$ and $\xi - M_{\tilde{\chi}_1^0}$ plane, respectively.

We observe that the invisible branching fraction can reach ∼10% for a LSP in the range $M_{\tilde{\chi}_1^0} \sim 7$–$23$ GeV. These scenarios are associated with NSDM with $\xi$ in the range ∼100–3000, as can be seen from Fig. 15(b) with the low values of $\xi$ being attained at low values of $M_{\tilde{\chi}_1^0}$. Typically $\mu \leq 500$ GeV to ensure a large enough coupling of the LSP to the $Z$ and thus a detectable SD rate which is dominated by the $Z$ exchange. The value of $\mu$ can, however, exceed 500 GeV when the LSP mass increases, $M_{\tilde{\chi}_1^0} \gtrsim 18$ GeV, since the Higgsino fraction of the LSP which drives its coupling to the $Z$ and Higgs is determined by $M_1$ and $\mu$. Moreover, the sensitivity of detectors also increases with the DM mass. For the parameter space points with $\mu \leq 500$ GeV, one could take advantage of the LSP mass determination at the ILC to clearly indicate that the DM candidate is a relic of nonstandard cosmology.

In a similar mass region for the LSP, we observe another interesting subgroup of parameter space points, which would be accessible to the future direct detection experiments only, namely, PICO-250 through the SD WIMP-proton based interactions and Xenon-nT through the SI WIMP-nucleon based interactions. We show these parameter space points in Fig. 16, in the $\xi - M_{\tilde{\chi}_1^0}$ plane. For these points, the Higgs invisible width is too small to be measured because of a slightly higher value for $\mu$. Still only a small fraction of these points correspond to $\mu > 500$ GeV, while most can be probed by ILC through the electroweakino searches. A detection in the Xenon-nT detector through the SI WIMP-nucleon based interaction and in PICO-250 through the SD WIMP-proton based interaction, complemented by detection in ILC through the electroweakino searches, for low $M_{\mathrm{DM}}$ ($M_{\mathrm{DM}} < 20$ GeV), would be indicative of a DM candidate which is a relic from nonstandard cosmology since the thermal relic density is roughly 2 orders of magnitude higher than the observed value of relic density.

Before concluding this subsection, we consider one last category of parameter space points, which can be probed by PICO-250 through the SD WIMP-proton based interactions and by ILC through the Higgs to invisible branching. All these parameter space points would also be sensitive to the electroweakino searches at ILC since $\mu \leq 500$ GeV. We show these parameter space points in the $\mathrm{Br}(h \to \tilde{\chi}_1^0\tilde{\chi}_1^0) - M_{\tilde{\chi}_1^0}$ and $\xi - M_{\tilde{\chi}_1^0}$ plane in Figs. 17(a) and 17(b), respectively. The color palette represents the value of $\mu$.

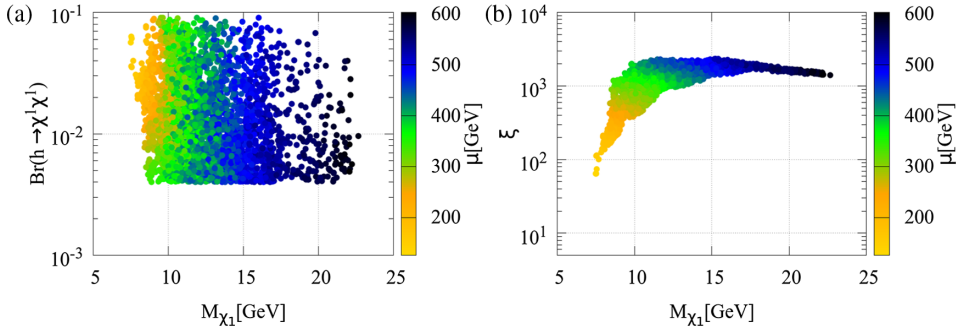


FIG. 15. (a) Scatter plot in the $\mathrm{Br}(h \to \tilde{\chi}_1^0\tilde{\chi}_1^0) - M_{\tilde{\chi}_1^0}$ plane and (b) in the $\xi - M_{\tilde{\chi}_1^0}$ plane for parameter space points which can be probed by PICO-250 through the SD WIMP-proton interactions, by Xenon-nT through the SI WIMP-nucleon based interactions, and also by ILC through the Higgs to invisible branching. The color palette corresponds to the value of the Higgsino mass parameter ($\mu$).

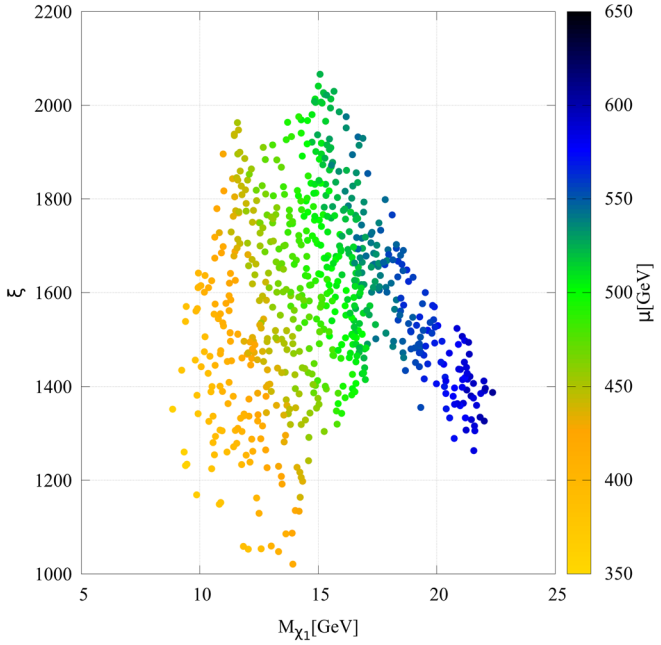


FIG. 16. Scatter plot in the $\xi - M_{\tilde{\chi}_1^0}$ plane for parameter space points which can be probed by PICO-250 through the SD WIMP-proton interactions and by Xenon-nT through the SI WIMP-nucleon based interactions. The color palette corresponds to the value of the Higgsino mass parameter ($\mu$).

The parameter space points are confined within $M_{\tilde{\chi}_1^0} \leq 10$ GeV and have $\xi \sim 70 - 2 \times 10^3$; therefore an observation within this scenario would reflect that the DM candidate ($\tilde{\chi}_1^0$) is an artifact of nonstandard cosmology.

### E. Detection at Xenon-nT and LZ

The parameter space points, which would be accessible to Xenon-nT through SI WIMP-nucleon based interactions and to LZ through SD WIMP-neutron based interactions only, have been shown in Fig. 18, in the $\xi - M_{\tilde{\chi}_1^0}$ plane. These parameter space points extend over $M_{\tilde{\chi}_1^0} \sim 22$–$62.5$ GeV, with $\xi$ varying between 0.02 and 2000. The parameter space can be split into three different regions: the nonresonant region ($M_{\tilde{\chi}_1^0} \lesssim 35$ GeV) where $\xi \sim 300$–$2000$, the $Z$-resonance region ($M_{\tilde{\chi}_1^0} \sim 35$–$55$ GeV) with $\xi \sim 3$–$200$, and the Higgs resonance region ($M_{\tilde{\chi}_1^0} \sim 55$–$62.5$ GeV), with $\xi$ varying between 0.02 and 60. A signal in DD and a rough determination of the DM mass in the first two regions would be indicative of the DM candidate being a relic from nonstandard cosmology. On the other hand, the observation of a DM mass in the Higgs resonance region would not be adequate enough to identify whether the DM candidate corresponds to the thermal picture or to a nonstandard cosmology.

We observe a small set of parameter space points in the Higgs resonance region which are sensitive to the electroweakino searches at ILC as well, $\mu \leq 500$ GeV, and these points all correspond to $\xi < 1$. Adding the precise information on the value of $M_{\tilde{\chi}_1^0}$ and $\mu$ from the ILC to an observation of a signal at Xenon-nT through the SI WIMP-nucleon based interactions and at LZ through the SD WIMP-neutron based interactions would indicate that the DM candidate ($\tilde{\chi}_1^0$) is a standard cosmological relic.

Another similar subcategory of parameter space points are observed that would be detectable at Xenon-nT (through the SI WIMP-nucleon based interactions), at LZ, and at ILC (through the Higgs to invisible branching). These points extend over the three mass regions discussed above but are associated with a value for $\xi$ lower by ∼1–2 orders of magnitude. This is a result of an increased coupling of the LSP to the Higgs and $Z$ bosons. Indeed, the majority of such parameter points have $\mu \leq 500$ GeV (shown in red in Fig. 19), therefore making them accessible to the electroweakino searches at ILC. With a very precise $M_{\tilde{\chi}_1^0}$ and a DM signal at Xenon-nT (through SI WIMP-nucleon based interactions), at LZ (through SD WIMP-neutron based interactions), and at ILC (through both electroweakino searches and Higgs to invisible branching fraction), one could conclude that the DM requires a nonstandard cosmology unless the LSP mass ($\tilde{\chi}_1^0$) lies in the Higgs resonance region.

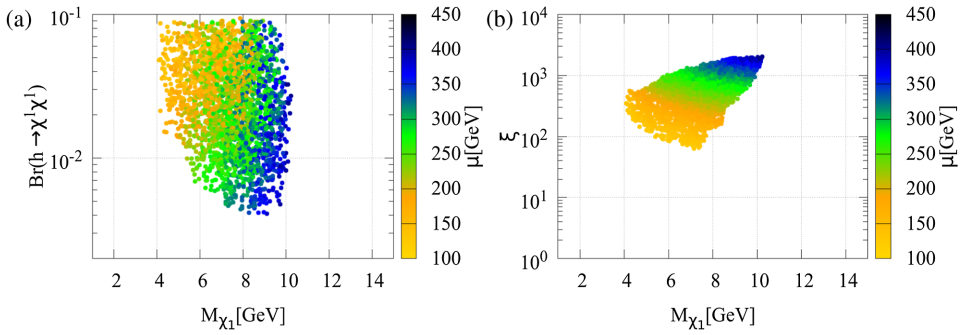


FIG. 17. (a) Scatter plot in the $\mathrm{Br}(h \to \tilde{\chi}_1^0 \tilde{\chi}_1^0) - M_{\tilde{\chi}_1^0}$ plane. (b) Scatter plot in the $\xi - M_{\tilde{\chi}_1^0}$ plane for parameter space points which can be probed by PICO-250 through the SD WIMP-proton interactions and also by ILC through the Higgs to invisible branching. The color palette corresponds to the value of the Higgsino mass parameter ($\mu$).

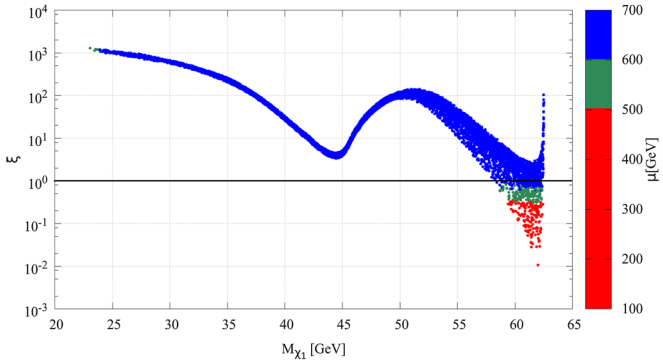


FIG. 18. Scatter plot in the $\xi - M_{\tilde{\chi}_1^0}$ plane for parameter space points which can be probed by LZ through the SD WIMP-neutron interactions and by Xenon-nT through the SI WIMP-nucleon based interactions. The color palette corresponds to the value of the Higgsino mass parameter ($\mu$).

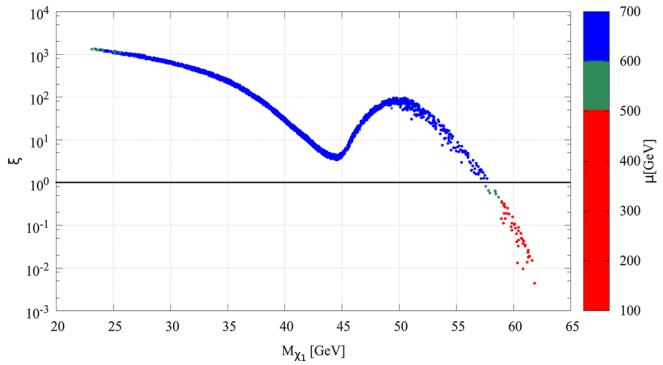


FIG. 19. Scatter plot in the $\xi - M_{\tilde{\chi}_1^0}$ plane for parameter space points which can be probed by LZ through the SD WIMP-neutron interactions, by Xenon-nT through the SI WIMP-nucleon based interactions and by ILC through the Higgs to invisible branching fraction. The color palette corresponds to the value of the Higgsino mass parameter ($\mu$).

### F. Scenarios probed at Xenon-nT, PICO-250, LZ, and ILC

In this subsection, we analyze those parameter space points which would be detectable at all the future direct detection experiments considered in this analysis, namely, Xenon-nT (through SI WIMP-nucleon based interactions), PICO-250 (through SD WIMP-proton based interactions), LZ (through the SD WIMP-neutron based interactions), and would also be accessible at ILC through the Higgs to invisible branching fraction and in some cases through electroweakino searches. We show these parameter space points in Fig. 20 in the $\xi - M_{\tilde{\chi}_1^0}$ plane. These parameter space points extend over a wide mass range $M_{\tilde{\chi}_1^0} \sim 7$–$62.5$ GeV, accompanied with a significant variation in $\xi$ as well, $\xi \sim 0.005$–$3000$.

The unique feature of this particular scenario is the presence of parameter space points in the $Z$ resonance region ($m_{\rm LSP} \approx 45$ GeV) with relic density $\Omega h^2 \leq 0.122$,

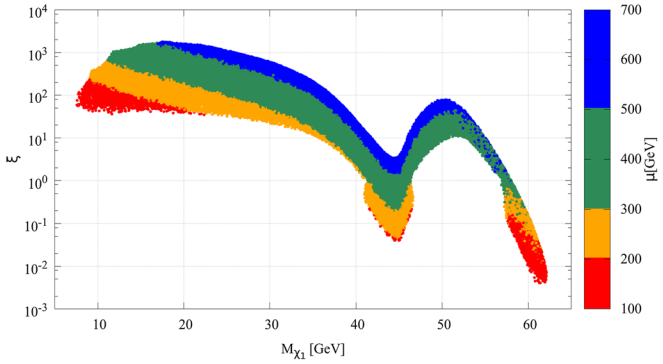


FIG. 20. Scatter plot in the $\xi - M_{\tilde{\chi}_1^0}$ plane for parameter space points which can be probed by PICO-250 through the SD WIMP-proton interactions, by LZ through the SD WIMP-neutron interaction, by Xenon-nT through the SI WIMP-nucleon based interactions, and also by ILC through the Higgs to invisible branching fraction. The color palette corresponds to the value of the Higgsino mass parameter ($\mu$).

which were absent in all other scenarios considered in this section. In addition, all such points have $\mu \leq 500$ GeV and are thus detectable through electroweakino searches at ILC as well. However, within the same $Z$ resonance region, we also found parameter points with $\mu < 500$ GeV for which $\xi > 1$. As a result, it would not be possible to identify whether a signal in the $Z$ resonance region is a signature of standard or nonstandard cosmology. Such a conclusion could, however, be reached for other mass ranges using the information on $M_{\tilde{\chi}_1^0}$ and $\mu$.

In Fig. 21, we show the parameter space points in the $\sigma_{\rm SI} - \xi$ plane, with $M_{\tilde{\chi}_1^0}$ represented through a color palette. The grey colored points correspond to those with $\mu > 500$ GeV while those represented through the color palette have $\mu \leq 500$ GeV, making them accessible to ILC through the electroweakino searches as well. The additional

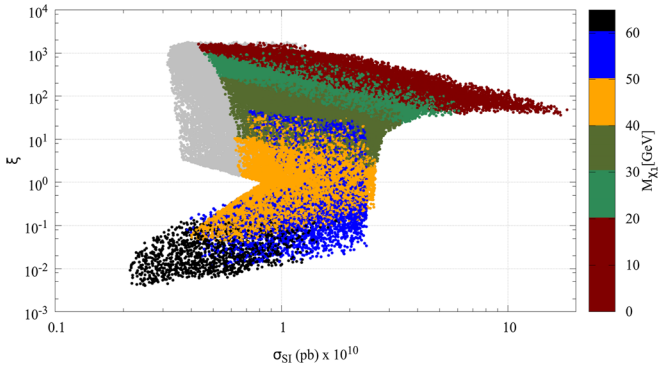


FIG. 21. Scatter plot in the $\sigma_{SI} - \xi$ plane for parameter space points which can be probed by PICO-250 through the SD WIMP-proton interactions, by LZ through the SD WIMP-neutron interaction, by Xenon-nT through the SI WIMP-nucleon based interactions, and also by ILC through the Higgs to invisible branching fraction. The color palette corresponds to the value of the LSP mass ($M_{\tilde{\chi}_1^0}$).

information from the determination of the LSP mass could be used to differentiate thermal and NSDM cosmological scenarios. For example, parameter space points in the mass range $M_{\tilde{\chi}_1^0} \leq 20$ GeV (shown in brown) are indicative of the DM candidate being an artifact of nonstandard cosmology. Another interesting mass region corresponds to $M_{\tilde{\chi}_1^0} > 60$ GeV (shown in black), which is confined to the region with $\xi < 1$ and is, hence, indicative of a DM candidate which is a relic from standard cosmology. It is not possible to make similar arguments for the $Z$ resonance region, where parameter points with both $\Omega h^2 > 0.122$ and $\Omega h^2 \leq 0.122$ are found. We found that the additional information from $\sigma_{\rm SD}$ measurements did not help to further constrain the parameter space.

## VII. PROSPECTS FOR HIGH LUMINOSITY LHC

In this section, we evaluate the role of the future runs of the LHC, with an integrated luminosity up to 3000 fb$^{-1}$, in probing the light neutralino DM model. We also briefly discuss certain unique signatures, which have a very negligible SM background and could be used to obtain information on the gaugino sector of the MSSM which would otherwise be difficult to access at ILC.

We begin by reminding ourselves of the following observation. It was seen in Secs. IV and V that the allowed parameter space was restricted to $\mathrm{Br}(h \to \tilde{\chi}_1^0\tilde{\chi}_1^0) \lesssim 10\%$, due to the imposition of the Higgs signal strength constraints, derived by CMS and ATLAS through a combined analysis of the 7 and 8 TeV LHC data [3]. Hence the projected LHC limits on $\mathrm{Br}(h \to \mathrm{invi})$ mentioned in the Introduction are not expected to imply any additional restriction on the allowed parameter space. Future prospects of chargino neutralino searches have been studied in [119] in the context of a high luminosity LHC run (300 fb$^{-1}$, 3000 fb$^{-1}$). In [119], the LSP ($\tilde{\chi}_1^0$) has been assumed to be binolike, while $\tilde{\chi}_2^0$ and $\tilde{\chi}_1{}^{\pm}$ have been assumed to be winolike and degenerate in mass. Upper limits have been derived on the mass of $\tilde{\chi}_2^0$ and $\tilde{\chi}_1{}^{\pm}$ as a function of $M_{\tilde{\chi}_1^0}$. For the three lepton final state from the $WZ$ mediated simplified model, the exclusion contour goes up to ∼1110 GeV, while the $5\sigma$ discovery contour reaches 820 GeV, for 3000 fb$^{-1}$ of integrated luminosity (see Fig. 4 of [119]). In the $Wh$ simplified scenario, the exclusion contour reaches 940 GeV, while the $5\sigma$ discovery contour reaches 650 GeV for 3000 fb$^{-1}$ of integrated luminosity [see Fig. 5(a) of [119]]. Thus the LHC will probe models with a gaugino mass of the order of the TeV scale in the case $M_2 < \mu$. Keeping these future projections in mind, we choose a representative benchmark point (BP 1) from the allowed parameter space with a chargino mass within the projected LHC exclusion limits. However, we do not demand the chargino to be winolike. We intentionally choose BP 1 to be such a parameter space point which evades detection from all the future DD experiments considered in our analysis, namely, Xenon-nT, PICO-250, and LZ, and also has $\mathrm{Br}(h \to \tilde{\chi}_1^0\tilde{\chi}_1^0) = 0.35\%$, making it inaccessible to the ILC through the Higgs to invisible searches. However, ino searches at ILC will be able to probe BP 1 (since $\mu = 442$ GeV). BP 1 corresponds to the following set of input parameters:

$$\begin{aligned}
M_1 &= 10.6\ \text{GeV}, & M_2 &= 812.6\ \text{TeV}, & \tan\beta &= 42.8, & \mu &= 442\ \text{TeV},\\
m_{\tilde{Q}_{3l}} &= 8.42\ \text{TeV}, & m_{\tilde{t}_R} &= 3.42\ \text{TeV}, & m_{\tilde{b}_R} &= 4.93\ \text{TeV}, & M_3 &= 4.36\ \text{TeV},\\
A_t &= 2.42\ \text{TeV}, & A_b &= 0\ \text{TeV} = A_\tau, & & & & \\
m_{\tilde{Q}_{2l,1l}} &= 3.00\ \text{TeV}, & m_{\tilde{c,u}_R} &= 3.00\ \text{TeV}, & m_{\tilde{s,d}_R} &= 3.00\ \text{TeV}, & m_{\text{slepton}} &= 3\ \text{TeV}.
\end{aligned} \tag{7.1}$$

BP 1 is characterized by a heavy wino component ($M_2 = 812.2$ GeV), resulting in nearly degenerate wino-type $\tilde{\chi}_4^0$ ($M_{\tilde{\chi}_4^0} = 822.81$ GeV) and $\tilde{\chi}_2{}^{\pm}$ ($M_{\tilde{\chi}_2{}^{\pm}} = 822.83$ GeV). The LSP ($\tilde{\chi}_1^0$) has a dominant bino fraction with mass $M_{\tilde{\chi}_1^0} = 10.3$ GeV. The Higgsino mass parameter ($\mu$) lies at an intermediate value of 442 GeV resulting in $\tilde{\chi}_2^0, \tilde{\chi}_3^0, \tilde{\chi}_1{}^{\pm}$ being dominantly Higgsino-type with masses, $M_{\tilde{\chi}_2^0} = 436.2$ GeV, $M_{\tilde{\chi}_3^0} = -446.4$ GeV, $M_{\tilde{\chi}_1{}^{\pm}} = 436.0$ GeV, and thus accessible at the ILC. At the LHC, the production cross section of winos is large and specific signatures can be found in the cascade decay of the directly produced wino-type chargino/neutralino pairs, $pp \to \tilde{\chi}_4^0\tilde{\chi}_2{}^{\pm}$. The cascade decay of the wino-type $\tilde{\chi}_4^0, \tilde{\chi}_2{}^{\pm}$ will be through the intermediate Higgsino-type inos. One such final state topology would be the $ZZWh + \not{E}_{\rm T}$ final state, resulting from a cascade decay of the form $\tilde{\chi}_4^0 \to \tilde{\chi}_2^0 + Z$, $\tilde{\chi}_2^0 \to \tilde{\chi}_1^0 + h$ and $\tilde{\chi}_2^+ \to \tilde{\chi}_1^+ + Z, \tilde{\chi}_1^+ \to \tilde{\chi}_1^0 + W^+$. Summing up all possible decay modes of the $\tilde{\chi}_4^0, \tilde{\chi}_2{}^{\pm}$ pair, which end up in the $ZZWh + \not{E}_{\rm T}$ final state, we obtain a total branching of ∼15%. Considering the direct pair production cross section, $\sigma(pp \to \tilde{\chi}_4^0\tilde{\chi}_2{}^{\pm}) \sim 3$ fb, evaluated using PROSPINO for $\sqrt{s} = 14$ TeV, we expect to produce ∼1350 events in the channel $pp \to \tilde{\chi}_4^0\tilde{\chi}_2{}^{\pm} \to ZZWh + \not{E}_{\rm T}$ at LHC for 3000 fb$^{-1}$ of integrated luminosity. Numerous other final states of the form $VVVW + \not{E}_{\rm T}$ or $VWWW + \not{E}_{\rm T}$ ($V = Z, h$) are also possible; all have a minimal SM background.

For example, the $ZZWh + \not{E}_T$ final state could be examined in the $5l + b\bar{b} + \not{E}_T$ channel, which has a negligible standard model background. The observation of a signal in these search channels, besides giving precious information on the hierarchy of the neutralino/chargino masses, would open the possibility of obtaining some rough estimate of $M_2$ from mass difference measurements. In addition, the ILC will be able to perform very precise measurements of $\mu$ and $M_{\tilde{\chi}_1^0}$ for BP1. For this benchmark, this information coupled with the nonobservation of light sfermions at the LHC and ILC will be sufficient to establish that the neutralino LSP cannot be a thermal DM candidate. In general, and especially for LSP with masses near $m_h/2$, the determination of only three parameters of the gaugino sector is not sufficient to establish whether the neutralino LSP observed is a thermal DM candidate or one needs to appeal to a nonstandard cosmological model. In particular, information on the fourth parameter, $\tan\beta$, is needed. In favorable circumstances it could be extracted from pseudoscalar searches especially if its value is large. Recall that the pseudoscalar production cross section in the $b\bar{b}A$ mode is directly proportional to $(\tan\beta)^2$. A detailed investigation of relic density reconstruction is beyond the scope of this work.

## VIII. CONCLUSION

We have revisited the case of the light neutralino DM in supersymmetry and investigated the impact of a precise measurement of the Higgs invisible width on the allowed parameter space of the pMSSM where only electroweakinos and the third generation fermions are allowed to be below 2 TeV. In the standard cosmological scenario where the neutralino is in thermal equilibrium with SM in the early universe, the light neutralino is confined to two narrow ranges of masses around $m_Z/2$ and $m_h/2$. Both regions will be probed entirely by the Xenon-1T direct detection experiment while only the first region can be entirely probed by a precise measurement of the Higgs invisible width achievable at the future ILC. Direct searches for Higgsino at the ILC will allow one to cover partly the Higgs funnel region. These conclusions are based on the assumption that there can be another DM component to explain the relic density when the neutralino DM is found to be underabundant. This approach is rather conservative since if we instead invoke a nonthermal mechanism to bring the low relic density scenarios within the PLANCK range, constraints from direct detection become more severe and only a small fraction passes the constraint from LUX.

The picture changes completely once we relax the relic density constraint by assuming that some nonstandard mechanism enhances the total entropy density by the late decay of a field to SM fields. The allowed range of masses for the neutralino LSP extends to $\sim$1 GeV, and it becomes much more difficult to cover the full parameter space with SI direct detection. SD experiments such as LZ and PICO-250 can in principle extend the reach, especially for DM masses below 10 GeV. However, the expected cross sections for such low masses of the LSP in this case can be below the coherent neutrino scattering limit and therefore unreachable by these detectors. Therefore, a precise measurement of the Higgs width is extremely important and in several cases provides the only handle on the LSP.

In the event of a discovery, the complementary measurements of Higgs invisible width or new particles at colliders and of DM direct detection can shed light not just on the nature of the DM but also on the cosmological scenario, in some cases pointing necessarily toward nonstandard mechanisms for DM production. Various combinations of measurements can potentially point to a particular region of parameter space. For example, observation of a signal at Xenon-nT, combined with the observation of the LSP and of Higgsinos of mass below 500 GeV at the ILC, would imply that compatibility with the MSSM can only be accommodated for two precise mass regions, one with $M_\chi \approx 10$ GeV and the other with $M_\chi \approx 60$ GeV. Moreover, the first region can be consistent with only a nonthermal mechanism while the second can be compatible with a thermal relic.

We expect that the searches for electroweakinos at the LHC 13 TeV will contribute to constraining the parameter space but scenarios with $\mu, M_2$ at the TeV scale will remain out of reach. In the optimistic case, where we have winos lying below 800 GeV, and Higgsinos lighter than the wino, there are spectacular signatures like $4V(= W/Z/h) + \not{p}_T$, which are background free and can readily be observed at the high luminosity LHC. In this case a rough value of $M_2$ can potentially be extracted while a precise value of $\mu$ and $M_1$ can be extracted from Higgsino searches at the ILC if $\mu$ is less than 500 GeV. However, even in the optimistic scenario, where the above parameters are measured to some degree of accuracy, the value of the relic density can be restricted only within a certain range due to the lack of measurements of other parameters of the model.

In summary, measurements at the ILC and in direct detection measurements will provide the most important hints in determining the precise nature of the light neutralino and could elucidate the cosmological nature of the light neutralino dark matter.

## ACKNOWLEDGMENTS

This work is supported by the "Investissements d'avenir, Labex ENIGMASS," by the French ANR, Projects No. DMAstro-LHC and No. ANR-12-BS05-006, by the CNRS LIA (Laboratoire International Associé) THEP (Theoretical High Energy Physics), and by the INFRE-HEPNET (IndoFrench Network on High Energy Physics) of CEFIPRA/IFCPAR (Indo-French Centre for the Promotion of Advanced Research). The work of B. B. is supported by the Department of Science and Technology,

Government of India, under the Grant Agreement No. IFA13-PH-75 (INSPIRE Faculty Award). The work of R. M. G. is supported by the Department of Science and Technology, India under Grant No. SR/S2/JCB-64/2007. R. M. G. and B. B. acknowledge hospitality at LAPTh where part of this work was carried out. The work of D. S. is supported by the National Science Foundation under Grant No. PHY-1519045.

[1] G. Aad *et al.* (ATLAS Collaboration), Observation of a new particle in the search for the Standard Model Higgs boson with the ATLAS detector at the LHC, Phys. Lett. B **716**, 1 (2012).
[2] S. Chatrchyan *et al.* (CMS Collaboration), Observation of a new boson at a mass of 125 GeV with the CMS experiment at the LHC, Phys. Lett. B **716**, 30 (2012).
[3] G. Aad *et al.* (ATLAS and CMS Collaborations), Measurements of the Higgs boson production and decay rates and constraints on its couplings from a combined ATLAS and CMS analysis of the LHC $pp$ collision data at $\sqrt{s} = 7$ and 8 TeV, J. High Energy Phys. 08 (2016) 045.
[4] J. F. Gunion, Detecting an Invisibly Decaying Higgs Boson at a Hadron Supercollider, Phys. Rev. Lett. **72**, 199 (1994).
[5] D. Choudhury and D. P. Roy, Signatures of an invisibly decaying Higgs particle at LHC, Phys. Lett. B **322**, 368 (1994).
[6] O. J. P. Eboli and D. Zeppenfeld, Observing an invisible Higgs boson, Phys. Lett. B **495**, 147 (2000).
[7] R. M. Godbole, M. Guchait, K. Mazumdar, S. Moretti, and D. P. Roy, Search for "invisible" Higgs signals at LHC via associated production with gauge bosons, Phys. Lett. B **571**, 184 (2003).
[8] H. Davoudiasl, T. Han, and H. E. Logan, Discovering an invisibly decaying Higgs at hadron colliders, Phys. Rev. D **71**, 115007 (2005).
[9] E. Accomando *et al.*, Workshop on *CP* Studies and Non-Standard Higgs Physics, arXiv:hep-ph/0608079.
[10] Y. Bai, P. Draper, and J. Shelton, Measuring the invisible Higgs width at the 7 and 8 TeV LHC, J. High Energy Phys. 07 (2012) 192.
[11] A. Djouadi, A. Falkowski, Y. Mambrini, and J. Quevillon, Direct detection of Higgs-portal dark matter at the LHC, Eur. Phys. J. C **73**, 2455 (2013).
[12] D. Ghosh, R. Godbole, M. Guchait, K. Mohan, and D. Sengupta, Looking for an invisible Higgs signal at the LHC, Phys. Lett. B **725**, 344 (2013).
[13] C. Bernaciak, T. Plehn, P. Schichtel, and J. Tattersall, Spying an invisible Higgs boson, Phys. Rev. D **91**, 035024 (2015).
[14] S. Chatrchyan *et al.* (CMS Collaboration), Search for invisible decays of Higgs bosons in the vector boson fusion and associated ZH production modes, Eur. Phys. J. C **74**, 2980 (2014).
[15] CMS Collaboration, Searches for invisible Higgs boson decays with the CMS detector, CERN Technical Report No. CMS-PAS-HIG-16-016, Geneva, 2016; https://cds.cern.ch/record/2201136.
[16] V. Khachatryan *et al.* (CMS Collaboration), Searches for invisible decays of the Higgs boson in $pp$ collisions at $\sqrt{(s)} = 7$, 8, and 13 TeV, J. High Energy Phys. 02 (2017) 135.
[17] G. Aad *et al.* (ATLAS Collaboration), Constraints on new phenomena via Higgs boson couplings and invisible decays with the ATLAS detector, J. High Energy Phys. 11 (2015) 206.
[18] G. Aad *et al.* (ATLAS Collaboration), Search for invisible decays of a Higgs boson using vector-boson fusion in $pp$ collisions at $\sqrt{s} = 8$ TeV with the ATLAS detector, J. High Energy Phys. 01 (2016) 172.
[19] S. Dawson *et al.*, Working group report: Higgs boson, arXiv:1310.8361.
[20] M. Zanetti (on behalf of ATLAS and CMS Collaborations), Prospects for precision Higgs physics with ATLAS and CMS at High Luminosity LHC, Report No. HC2013, Freiburg, 2013; https://indico.cern.ch/event/253774/contributions/567148/attachments/443067/614582/HiggsCouplingsProjections_HLLHC.pdf.
[21] N. Smith (on behalf of CMS Collaboration), Invisible Higgs decays, Report No. HC2016, 2016; https://indico.cern.ch/event/477407/contributions/2305073/attachments/1369949/2077172/nsmith_hc16_zhinv.pdf.
[22] K. Peters, Prospects for beyond Standard Model Higgs boson searches at future LHC runs and other machines, arXiv:1701.05124.
[23] CMS Collaboration, Updates on projections of physics reach with the upgraded CMS detector for high luminosity LHC, https://cds.cern.ch/record/2221747.
[24] G. Belanger, B. Dumont, U. Ellwanger, J. F. Gunion, and S. Kraml, Status of invisible Higgs decays, Phys. Lett. B **723**, 340 (2013).
[25] D. M. Asner *et al.*, ILC Higgs White Paper, arXiv:1310.0763.
[26] K. Griest and H. E. Haber, Invisible decays of Higgs bosons in supersymmetric models, Phys. Rev. D **37**, 719 (1988).
[27] A. Djouadi, P. Janot, J. Kalinowski, and P. M. Zerwas, SUSY decays of Higgs particles, Phys. Lett. B **376**, 220 (1996).
[28] G. Belanger, F. Boudjema, F. Donato, R. Godbole, and S. Rosier-Lees, SUSY Higgs at the LHC: Effects of light charginos and neutralinos, Nucl. Phys. **B581**, 3 (2000).
[29] G. Belanger, F. Boudjema, A. Cottrant, R. M. Godbole, and A. Semenov, The MSSM invisible Higgs in the light of dark matter and g-2, Phys. Lett. B **519**, 93 (2001).
[30] G. Belanger, F. Boudjema, A. Cottrant, A. Pukhov, and S. Rosier-Lees, Lower limit on the neutralino mass in the general MSSM, J. High Energy Phys. 03 (2004) 012.

[31] L. Calibbi, T. Ota, and Y. Takanishi, Light neutralino in the MSSM: A playground for dark matter, flavor physics and collider experiments, J. High Energy Phys. 07 (2011) 013.
[32] H. K. Dreiner, J. S. Kim, and O. Lebedev, First LHC constraints on neutralinos, Phys. Lett. B **715**, 199 (2012).
[33] B. Ananthanarayan, J. Lahiri, P. N. Pandita, and M. Patra, Invisible decays of the lightest Higgs boson in supersymmetric models, Phys. Rev. D **87**, 115021 (2013).
[34] L. Calibbi, J. M. Lindert, T. Ota, and Y. Takanishi, Cornering light neutralino dark matter at the LHC, J. High Energy Phys. 10 (2013) 132.
[35] G. Belanger, G. D. La Rochelle, B. Dumont, R. M. Godbole, S. Kraml, and S. Kulkarni, LHC constraints on light neutralino dark matter in the MSSM, Phys. Lett. B **726**, 773 (2013).
[36] T. Han, Z. Liu, and S. Su, Light neutralino dark matter: Direct/indirect detection and collider searches, J. High Energy Phys. 08 (2014) 093.
[37] G. Belanger, D. Ghosh, R. Godbole, and S. Kulkarni, Light stop in the MSSM after LHC Run 1, J. High Energy Phys. 09 (2015) 214.
[38] K. Hamaguchi and K. Ishikawa, Prospects for Higgs- and $Z$-resonant neutralino dark matter, Phys. Rev. D **93**, 055009 (2016).
[39] O. Buchmueller *et al.*, Frequentist analysis of the parameter space of minimal supergravity, Eur. Phys. J. C **71**, 1583 (2011).
[40] H. Baer, V. Barger, and A. Mustafayev, Neutralino dark matter in mSUGRA/CMSSM with a 125 GeV light Higgs scalar, J. High Energy Phys. 05 (2012) 091.
[41] C. Strege, G. Bertone, F. Feroz, M. Fornasa, R. Ruiz de Austri, and R. Trotta, Global fits of the cMSSM and NUHM including the LHC Higgs discovery and new XENON100 constraints, J. Cosmol. Astropart. Phys. 04 (2013) 013.
[42] D. Ghosh, M. Guchait, S. Raychaudhuri, and D. Sengupta, How constrained is the cMSSM?, Phys. Rev. D **86**, 055007 (2012).
[43] L. Roszkowski, E. M. Sessolo, and A. J. Williams, What next for the CMSSM and the NUHM: Improved prospects for superpartner and dark matter detection, J. High Energy Phys. 08 (2014) 067.
[44] O. Buchmueller, M. Citron, J. Ellis, S. Guha, J. Marrouche, K. A. Olive, K. de Vries, and J. Zheng, Collider interplay for supersymmetry, Higgs and dark matter, Eur. Phys. J. C **75**, 469 (2015); Erratum, Eur. Phys. J. C **76**, 190(E) (2016).
[45] P. Bechtle *et al.*, Killing the cMSSM softly, Eur. Phys. J. C **76**, 96 (2016).
[46] H. Baer, V. Barger, and H. Serce, SUSY under siege from direct and indirect WIMP detection experiments, Phys. Rev. D **94**, 115019 (2016).
[47] J. Ellis, J. L. Evans, A. Mustafayev, N. Nagata, and K. A. Olive, The Super-GUT CMSSM revisited, Eur. Phys. J. C **76**, 592 (2016).
[48] D. Hooper and T. Plehn, Supersymmetric dark matter: How light can the LSP be?, Phys. Lett. B **562**, 18 (2003).
[49] A. Bottino, N. Fornengo, and S. Scopel, Light relic neutralinos, Phys. Rev. D **67**, 063519 (2003).
[50] D. A. Vasquez, G. Belanger, C. Boehm, A. Pukhov, and J. Silk, Can neutralinos in the MSSM and NMSSM scenarios still be light?, Phys. Rev. D **82**, 115027 (2010).
[51] D. Feldman, Z. Liu, and P. Nath, Low mass neutralino dark matter in the MSSM with constraints from $B_s \to \mu^+\mu^-$ and Higgs search limits, Phys. Rev. D **81**, 117701 (2010).
[52] P. Grothaus, M. Lindner, and Y. Takanishi, Naturalness of neutralino dark matter, J. High Energy Phys. 07 (2013) 094.
[53] S. Profumo and T. Stefaniak, Alignment without decoupling: The portal to light dark matter in the MSSM, Phys. Rev. D **94**, 095020 (2016).
[54] H. K. Dreiner, S. Heinemeyer, O. Kittel, U. Langenfeld, A. M. Weber, and G. Weiglein, Mass bounds on a very light neutralino, Eur. Phys. J. C **62**, 547 (2009).
[55] D. A. Vasquez, G. Belanger, and C. Boehm, Revisiting light neutralino scenarios in the MSSM, Phys. Rev. D **84**, 095015 (2011).
[56] A. Arbey, M. Battaglia, and F. Mahmoudi, Supersymmetry with light dark matter confronting the recent CDMS and LHC results, Phys. Rev. D **88**, 095001 (2013).
[57] A. Choudhury and A. Datta, Neutralino dark matter confronted by the LHC constraints on electroweak SUSY signals, J. High Energy Phys. 09 (2013) 119.
[58] A. Fowlie, K. Kowalska, L. Roszkowski, E. M. Sessolo, and Y.-L. S. Tsai, Dark matter and collider signatures of the MSSM, Phys. Rev. D **88**, 055012 (2013).
[59] M. Cahill-Rowley, J. L. Hewett, A. Ismail, and T. G. Rizzo, Lessons and prospects from the pMSSM after LHC Run I, Phys. Rev. D **91**, 055002 (2015).
[60] L. Calibbi, J. M. Lindert, T. Ota, and Y. Takanishi, LHC tests of light neutralino dark matter without light sfermions, J. High Energy Phys. 11 (2014) 106.
[61] J. Bramante, N. Desai, P. Fox, A. Martin, B. Ostdiek, and T. Plehn, Towards the final word on neutralino dark matter, Phys. Rev. D **93**, 063525 (2016).
[62] G. Ricciardi *et al.*, Flavour, electroweak symmetry breaking and dark matter: State of the art and future prospects, Eur. Phys. J. Plus **130**, 209 (2015).
[63] E. J. Chun, S. Jung, and J.-C. Park, Very degenerate Higgsino dark matter, J. High Energy Phys. 01 (2017) 009.
[64] J. Cao, Y. He, L. Shang, W. Su, and Y. Zhang, Testing the light dark matter scenario of the MSSM at the LHC, J. High Energy Phys. 03 (2016) 207.
[65] M. Badziak, M. Olechowski, and P. Szczerbiak, Is well-tempered neutralino in MSSM still alive after 2016 LUX results?, arXiv:1701.05869.
[66] M. Beneke, A. Bharucha, F. Dighera, C. Hellmann, A. Hryczuk, S. Recksiegel, and P. Ruiz-Femenia, Relic density of wino-like dark matter in the MSSM, J. High Energy Phys. 03 (2016) 119.
[67] C. Boehm, P. S. B. Dev, A. Mazumdar, and E. Pukartas, Naturalness of light neutralino dark matter in pMSSM after LHC, XENON100 and Planck data, J. High Energy Phys. 06 (2013) 113.
[68] T. Moroi and L. Randall, Wino cold dark matter from anomaly mediated SUSY breaking, Nucl. Phys. **B570**, 455 (2000).

[69] G. B. Gelmini and P. Gondolo, Neutralino with the right cold dark matter abundance in (almost) any supersymmetric model, Phys. Rev. D **74**, 023510 (2006).
[70] R. Allahverdi, B. Dutta, and K. Sinha, Successful supersymmetric dark matter with thermal over/under-abundance from late decay of a visible sector scalar, Phys. Rev. D **87**, 075024 (2013).
[71] H. Baer, K.-Y. Choi, J. E. Kim, and L. Roszkowski, Dark matter production in the early Universe: Beyond the thermal WIMP paradigm, Phys. Rep. **555**, 1 (2015).
[72] L. Aparicio, M. Cicoli, B. Dutta, S. Krippendorf, A. Maharana, F. Muia, and F. Quevedo, Non-thermal CMSSM with a 125 GeV Higgs, J. High Energy Phys. 05 (2015) 098.
[73] L. Aparicio, B. Dutta, M. Cicoli, F. Muia, and F. Quevedo, Light Higgsino dark matter from non-thermal cosmology, J. High Energy Phys. 11 (2016) 038.
[74] L. Roszkowski, S. Trojanowski, and K. Turzynski, Understanding the thermal history of the Universe through direct and indirect detection of dark matter, arXiv:1703.00841.
[75] V. Khachatryan *et al.* (CMS Collaboration), Search for neutral MSSM Higgs bosons decaying to a pair of tau leptons in $pp$ collisions, J. High Energy Phys. 10 (2014) 160.
[76] P. Bechtle, S. Heinemeyer, O. Stal, T. Stefaniak, and G. Weiglein, Probing the Standard Model with Higgs signal rates from the Tevatron, the LHC and a future ILC, J. High Energy Phys. 11 (2014) 039.
[77] R. Aaij *et al.* (LHCb Collaboration), First Evidence for the Decay $B_s^0 \to \mu^+\mu^-$, Phys. Rev. Lett. **110**, 021801 (2013).
[78] G. Aad *et al.* (ATLAS and CMS Collaborations), Combined Measurement of the Higgs Boson Mass in $pp$ Collisions at $\sqrt{s} = 7$ and 8 TeV with the ATLAS and CMS Experiments, Phys. Rev. Lett. **114**, 191803 (2015).
[79] A. Djouadi, J.-L. Kneur, and G. Moultaka, SuSpect: A Fortran code for the supersymmetric and Higgs particle spectrum in the MSSM, Comput. Phys. Commun. **176**, 426 (2007).
[80] G. Belanger, F. Boudjema, A. Pukhov, and A. Semenov, micrOMEGAs: Version 1.3, Comput. Phys. Commun. **174**, 577 (2006).
[81] G. Belanger, F. Boudjema, A. Pukhov, and A. Semenov, micrOMEGAs: A Program for calculating the relic density in the MSSM, Comput. Phys. Commun. **149**, 103 (2002).
[82] G. Belanger, F. Boudjema, A. Pukhov, and A. Semenov, micrOMEGAs4.1: Two dark matter candidates, Comput. Phys. Commun. **192**, 322 (2015).
[83] Y. Amhis *et al.*, Averages of $b$-hadron, $c$-hadron, and $\tau$-lepton properties as of summer 2016, arXiv:1612.07233.
[84] V. Khachatryan *et al.* (LHCb and CMS Collaborations), Observation of the rare $B_s^0 \to \mu^+\mu^-$ decay from the combined analysis of CMS and LHCb data, Nature (London) **522**, 68 (2015).
[85] G. Abbiendi *et al.* (OPAL Collaboration), Search for chargino and neutralino production at $\sqrt{s} =$ 192–209 GeV at LEP, Eur. Phys. J. C **35**, 1 (2004).
[86] S. Schael *et al.* (SLD Electroweak Group, DELPHI, ALEPH, SLD, SLD Heavy Flavour Group, OPAL, LEP Electroweak Working Group, L3 Collaborations), Precision electroweak measurements on the $Z$ resonance, Phys. Rep. **427**, 257 (2006).
[87] V. Khachatryan *et al.* (CMS Collaboration), Constraints on the Higgs boson width from off-shell production and decay to $Z$-boson pairs, Phys. Lett. B **736**, 64 (2014).
[88] ATLAS and CMS Collaborations, Measurements of the Higgs boson production and decay rates and constraints on its couplings from a combined ATLAS and CMS analysis of the LHC $pp$ collision data at $\sqrt{s} = 7$ and 8 TeV, CERN Technical Report No. ATLAS-CONF-2015-044, Geneva, 2015; http://cds.cern.ch/record/2052552.
[89] R. K. Barman, B. Bhattacherjee, A. Choudhury, D. Chowdhury, J. Lahiri, and S. Ray, Status of MSSM Higgs sector after ICHEP 2016, arXiv:1608.02573.
[90] B. Dumont, B. Fuks, S. Kraml, S. Bein, G. Chalons, E. Conte, S. Kulkarni, D. Sengupta, and C. Wymant, Toward a public analysis database for LHC new physics searches using MADANALYSIS 5, Eur. Phys. J. C **75**, 56 (2015).
[91] D. Dercks, N. Desai, J. S. Kim, K. Rolbiecki, J. Tattersall, and T. Weber, CheckMATE 2: From the model to the limit, arXiv:1611.09856.
[92] G. Aad *et al.* (ATLAS Collaboration), Search for supersymmetry at $\sqrt{s} = 13$ TeV in final states with jets and two same-sign leptons or three leptons with the ATLAS detector, Eur. Phys. J. C **76**, 259 (2016).
[93] G. Aad *et al.* (ATLAS Collaboration), Search for direct production of charginos and neutralinos in events with three leptons and missing transverse momentum in $\sqrt{s} =$ 8 TeV $pp$ collisions with the ATLAS detector, J. High Energy Phys. 04 (2014) 169.
[94] G. Aad *et al.* (ATLAS Collaboration), Search for direct production of charginos, neutralinos and sleptons in final states with two leptons and missing transverse momentum in $pp$ collisions at $\sqrt{s} = 8$ TeV with the ATLAS detector, J. High Energy Phys. 05 (2014) 071.
[95] B. Dumont, MadAnalysis 5 implementation of ATLAS-SUSY-2013-11: di-leptons plus MET, http://inspirehep.net/record/1326686/.
[96] M. Aaboud *et al.* (ATLAS Collaboration), Search for new phenomena in final states with an energetic jet and large missing transverse momentum in $pp$ collisions at $\sqrt{s} =$ 13 TeV using the ATLAS detector, Phys. Rev. D **94**, 032005 (2016).
[97] G. Aad *et al.* (ATLAS Collaboration), Search for pair-produced third-generation squarks decaying via charm quarks or in compressed supersymmetric scenarios in $pp$ collisions at $\sqrt{s} = 8$ TeV with the ATLAS detector, Phys. Rev. D **90**, 052008 (2014).
[98] D. Sengupta and G. Chalons, Madanalysis 5 implementation of the ATLAS monojet analysis documented in arXiv:1407.0608, Phys. Rev. D **90**, 052008 (2015).
[99] D. Sengupta, Madanalysis5 implementation of the ATLAS monojet and missing transverse momentum search documented in arXiv:1604.07773.
[100] J. Alwall, R. Frederix, S. Frixione, V. Hirschi, F. Maltoni, O. Mattelaer, H. S. Shao, T. Stelzer, P. Torrielli, and M. Zaro, The automated computation of tree-level and next-to-leading order differential cross sections, and their matching to parton shower simulations, J. High Energy Phys. 07 (2014) 079.

[101] T. Sjostrand, S. Mrenna, and P. Z. Skands, PYTHIA 6.4 Physics and Manual, J. High Energy Phys. 05 (2006) 026.
[102] M. Cacciari, G. P. Salam, and G. Soyez, FastJet User Manual, Eur. Phys. J. C **72**, 1896 (2012).
[103] J. de Favereau, C. Delaere, P. Demin, A. Giammanco, V. Lematre, A. Mertens, and M. Selvaggi (DELPHES 3 Collaboration), DELPHES 3, A modular framework for fast simulation of a generic collider experiment, J. High Energy Phys. 02 (2014) 057.
[104] W. Beenakker, R. Hopker, and M. Spira, PROSPINO: A program for the production of supersymmetric particles in next-to-leading order QCD, arXiv:hep-ph/9611232.
[105] A. L. Read, Presentation of search results: The CL(s) technique, J. Phys. G **28**, 2693 (2002).
[106] C. Arina, M. Chala, V. Martin-Lozano, and G. Nardini, Confronting SUSY models with LHC data via electroweakino production, J. High Energy Phys. 12 (2016) 149.
[107] ATLAS Collaboration, Search for supersymmetry at the high luminosity LHC with the ATLAS experiment, CERN Technical Report No. ATL-PHYS-PUB-2014-010, Geneva, 2014; https://cds.cern.ch/record/1735031.
[108] P. A. R. Ade *et al.* (Planck Collaboration), Planck 2015 results. XIII. Cosmological parameters, Astron. Astrophys. **594**, A13 (2016).
[109] M. Szydagis (for the LUX and LZ Collaborations), The present and future of searching for dark matter with LUX and LZ, arXiv:1611.05525.
[110] E. Aprile *et al.* (XENON Collaboration), Physics reach of the XENON1T dark matter experiment, J. Cosmol. Astropart. Phys. 04 (2016) 027.
[111] M. Benito, N. Bernal, N. Bozorgnia, F. Calore, and F. Iocco, Particle dark matter constraints: The effect of galactic uncertainties, J. Cosmol. Astropart. Phys. 02 (2017) 007.
[112] D. S. Akerib *et al.* (LUX Collaboration), Results on the Spin-Dependent Scattering of Weakly Interacting Massive Particles on Nucleons from the Run 3 Data of the LUX Experiment, Phys. Rev. Lett. **116**, 161302 (2016).
[113] P. Cushman *et al.*, Working Group Report: WIMP dark matter direct detection, arXiv:1310.8327.
[114] H. Baer, M. Berggren, J. List, M. M. Nojiri, M. Perelstein, A. Pierce, W. Porod, and T. Tanabe, Physics case for the ILC Project: Perspective from beyond the standard model, arXiv:1307.5248.
[115] G. Gelmini, P. Gondolo, A. Soldatenko, and C. E. Yaguna, Effect of a late decaying scalar on the neutralino relic density, Phys. Rev. D **74**, 083514 (2006).
[116] R. Agnese *et al.* (SuperCDMS Collaboration), Projected sensitivity of the SuperCDMS SNOLAB experiment, Phys. Rev. D **95**, 082002 (2017).
[117] Y. Li and A. Nomerotski, Chargino and neutralino masses at ILC, arXiv:1007.0698.
[118] M. Drees and C.-L. Shan, Model-independent determination of the WIMP mass from direct dark matter detection data, J. Cosmol. Astropart. Phys. 06 (2008) 012.
[119] ATLAS Collaboration, Searches for supersymmetry at the high luminosity LHC with the ATLAS detector, CERN Technical Report No. ATL-PHYS-PUB-2013-002, Geneva, 2013; https://cds.cern.ch/record/1512933.